SKI Report 2008:30

Research

A model for fission gas release from mixed oxide nuclear fuel

Lars Olof Jernkvist

December 2007

ISSN 1104-1374
ISRN SKI-R-08/30-SE

SKI

SKI Perspective

Nuclear fuel containing mixed oxide (MOX) pellets have been used since the 1960´s. MOX fuel pellets are made from a mixture of uranium and plutonium oxide. MOX allows the large quantities of fissile isotopes produced and remaining in spent nuclear fuel from light water reactors to be recycled. Producing MOX fuel can be seen as a method to more efficiently use the natural uranium since most isotopes in natural uranium are the Pu-producing U-238. In fact, programs for using MOX were developed in the 1970´s to meet the feared or anticipated scarce supply of uranium at moderate prices. Although uranium prices have remained moderate, MOX is used in nuclear power reactors in for example Belgium, Germany, France and Switzerland, while other countries like Japan have programs for introducing MOX as part of their nuclear fuel cycle.

SKI has recently identified a need to gain knowledge about the in-reactor performance of mixed oxide nuclear fuel. Since issues regarding the properties, manufacturing and transportation of MOX fuel occasionally attract the attention of media it may be of public interest to gain knowledge of its utilisation as well. Small quantities of fuel rods have been irradiated in Swedish reactors, and there exist plans for using limited quantities of MOX fuel in Swedish power plants in the near future.

In a previous project (SKI 2005/1089) basic physical properties and some models for fuel rods with MOX pellets were studied to allow comparing the use of MOX with conventional UO_2 fuel in light water reactors in a general sense. The present study covers computer models for fission product gas release and densification.

Responsible for the project at SKI has been Jan-Erik Lindbäck.
SKI reference: SKI 2006/1134

SKI Report 2008:30

Research

A model for fission gas release from mixed oxide nuclear fuel

Lars Olof Jernkvist

Quantum Technologies AB
Uppsala Science Park
SE-751 83 Uppsala
Sweden

December 2007

List of contents

Summary III
Sammanfattning IV

1 Introduction 1

2 Model description 5
2.1 Representation of MOX fuel material 5
2.2 Calculation of local fission rate and burnup 9
2.3 Calculation of local fuel composition 12
2.4 Calculation of fission gas release 15

3 Calibration and verification of the model 17
3.1 Database used for model calibration 17
3.2 Calibration method 19
3.3 Optimised model parameters 19
3.3.1 Extrapolated agglomerate radius 20
3.3.2 Fission gas diffusivity 20
3.3.3 Grain boundary gas saturation threshold 21

4 Results and discussion 23
4.1 Comparison of FRAPCON-3.3 fission gas release models 23
4.2 Calculated effect of MOX fuel heterogeneity on FGR 27
4.3 Calculated effect of heterogeneity on fuel densification 28
4.4 Discussion 31

5 Conclusions 33

6 References 35

List of appendices

Appendix A:
Assessment cases for MOX fuel fission gas release A-1
A.1 IFA-597.4/5/6/7 ..... A-1
A.2 IFA-606 ..... A-3
A.3 IFA-629.1 ..... A-5
A.4 IFA-648.1/629.3 ..... A-7

Appendix B:
Fuel densification model in FRAPCON-3.3 ..... B-1

Summary

This report deals with a computational model for release of gaseous fission products from mixed oxide (MOX) nuclear fuel with heterogeneous microstructure. The model treats fission gas release from plutonium-rich agglomerates and the plutonium-lean fuel matrix separately, thereby considering the differences in isotope composition, fission rate and burnup between the two phases. The mechanisms for gas release are, however, assumed to be identical for agglomerates and matrix, and a slightly modified form of the GRAGG model by Forsberg and Massih is applied to calculate the gas release for each phase of the fuel material. The total gas release from the heterogeneous MOX material is then calculated by weighting the contribution from each phase with respect to its volume fraction. The theoretical background to the model is presented in the report, and its implementation in SKI's version of the FRAPCON-3.3 fuel performance program is described.

Calculated fission gas release fractions compare favourably with measured data for six pressurized water reactor fuel rods, all of which were charged with mixed oxide fuel. The rods were tested in the Halden reactor, and instrumented with pressure transducers for on-line measurements of fuel fission gas release with respect to time under irradiation. The proposed model reproduces the measured data from these experiments more accurately than the standard gas release model for MOX fuel in FRAPCON-3.3.

Parametric studies with the proposed model confirm the general experience that MOX fuel fission gas release increases with increasing size of the plutonium-rich agglomerates. However, this trend is not seen for small agglomerates, and according to our computational model, the MOX fuel material can be viewed as homogeneous with regard to fission gas release when the agglomerate size is below a certain threshold. The calculated threshold size depends on fuel plutonium content and the distribution of plutonium between agglomerates and fuel matrix. For typical MIMAS AUC MOX fuel, the calculated agglomerate threshold size is about 15 μm.

Finally, in-reactor densification of heterogeneous MOX fuel is studied with a composite material approach, similar to the one used in the proposed fission gas release model. The calculated impact of MOX fuel heterogeneity on in-reactor densification is small. However, this conclusion is based on rough calculations with an empirical densification model in FRAPCON-3.3, and a more rigorous analysis is warranted to draw a firm conclusion on this issue.

Sammanfattning

Denna rapport behandlar en beräkningsmodell för frigörelse av gasformiga fissionsprodukter från plutoniumhaltigt kärnbränsle (MOX-bränsle) med heterogen mikrostruktur. Modellen hanterar gasfrigörelse från bränslets plutoniumrika agglomerat och dess plutoniumfattiga matrismaterial var för sig, med beaktande av skillnader i isotopsammansättning, fissionstäthet och utbränning mellan materialets två faser. Mekanismerna för gasfrigörelse antas emellertid vara desamma i agglomerat och matris, och en lätt modifierad variant av Forsberg och Massihs modell GRAGG används för att beräkna gasfrigörelsen från bränslets två faser. Den totala gasfrigörelsen från det heterogena MOX-bränslet bestäms genom att väga samman bidragen från faserna i proportion till deras volymsandelar. I rapporten presenteras teorin bakom modellen, och dess införande i SKI:s version av bränslestavprogrammet FRAPCON-3.3 beskrivs.

Beräknad fissionsgasfrigörelse överensstämmer väl med mätdata från sex bränslestavar av tryckvattenreaktortyp med MOX-bränsle. De beaktade bränslestavarna provades i Haldenreaktorn, och var utrustade med tryckgivare för mätning av fissionsgas-frigörelsen som funktion av tid under bränslets bestrålning i reaktorn. Den föreslagna modellen återspeglar mätdata med större noggrannhet än standardmodellen för gasfrigörelse från MOX-bränsle i FRAPCON-3.3.

Parameterstudier med den föreslagna modellen bekräftar det välkända faktum att fissionsgasfrigörelsen ökar i proportion till storleken hos de plutoniumrika agglomeraten hos MOX-bränslet. Detta samband är dock obefintligt för små agglomerat, och enligt vår beräkningsmodell kan MOX-bränslet betraktas som homogent med avseende på fissionsgasfrigörelse, då agglomeraten är mindre än ett visst tröskelvärde. Det beräknade tröskelvärdet beror av bränslets plutoniumhalt och fördelningen av plutonium mellan agglomerat och matris. För MOX-bränsle framställt genom MIMAS AUC-processen beräknas nämnda tröskelstorlek vara ungefär 15 μm.

Slutligen studeras förtätning (densifiering) av det heterogena MOX-bränslet under reaktordrift med hjälp av en kompositmaterialmodell av samma typ som i den föreslagna gasfrigörelsemodellen. Den beräknade inverkan av MOX-bränslets heterogenitet är liten. Denna slutsats baseras dock på överslagsberäkningar med en empirisk bränsleförtätningsmodell i FRAPCON-3.3, och en djupare analys är önskvärd för att bekräfta resultaten.

1 Introduction

Nuclear fuel for light water reactors (LWRs) consists of either uranium dioxide or a mixture of uranium and plutonium dioxide; the latter kind of fuel is known as mixed oxide (MOX) fuel. The MOX fuel typically contains about 5-7 wt% plutonium, which makes up the major part of fissile isotopes in the material.

Mixed oxide fuel is not as common as pure UO_2 fuel, but its use is gradually increasing. Today, MOX fuel is used in about forty light water reactors, most of which are of pressurized water reactor (PWR) design and located in Europe and Japan (IAEA, 2003). Operating experience from these reactors, and also from test reactors, shows that MOX fuel, under certain conditions, release more gaseous fission products than pure UO_2 fuel at comparable operating conditions, although the mechanisms for fission gas release are believed to be identical in the two materials (Massih, 2006). The higher fission gas release in MOX fuel can partly be explained by higher operating temperatures relative to UO_2 fuel, due to lower thermal conductivity of the MOX material. Moreover, the grains are often smaller in MOX than in UO_2 fuel, which may also contribute to the observed difference in fission gas release (Guerin et al., 2000).

Another possible explanation to the higher fission gas release is that the fissile material is heterogeneously distributed at a microscopic scale in the MOX material. The microstructure of MOX fuel is usually described as a matrix of almost pure UO_2, containing plutonium-rich agglomerates. The size distribution, number density and plutonium concentration of the agglomerates depend on the fabrication process of the fuel; see the review by Massih (2006) and references therein for descriptions of the microstructure for common MOX fuel materials. The heterogeneous microstructure is believed to enhance fission gas release, since it leads to a locally increased fission rate in the plutonium-rich agglomerates. The locally increased fission rate results in:

- A high local production rate of fission fragments in the agglomerates, which leads to onset of fission gas release earlier than in a homogeneous material.
- A local increase of fission gas diffusivity in the agglomerates, at least at normal fuel operating temperatures, which enhances diffusion controlled gas release. However, at temperatures exceeding 1700-1880 K, gas diffusion in uranium and plutonium dioxide is controlled by temperature rather than radiation effects, and the locally increased fission rate in the agglomerates is less important (Ishida & Korei, 1994).
- A local temperature increase in the agglomerates, which in turn promotes gas diffusivity. The effect is probably weak, since both analytical and numerical models suggest that the agglomerate temperature is increased by at most a few kelvin (Walker et al., 1997) and (Sauer & Besenböck, 2007).
- A different rate of densification and swelling for the agglomerates, in relation to the surrounding matrix material. Heterogeneous MOX fuel may crack due to the differential deformation, and the cracks provide release paths for the fission gas (Billaux & van Vliet, 1986).

- A high local burnup in the agglomerates, which means that the material within the plutonium-rich agglomerates undergoes re-structuring at fairly low pellet average burnup. The re-structuring is characterized by grain subdivision, increase in porosity and depletion of fission gas from the fuel material (Matzke, 1995) and (Spino et al., 1996). The resulting microstructure, usually referred to as 'high burnup structure' or 'rim zone structure', is very porous and believed to enhance fission gas release (Jernkvist & Massih, 2002).

From these arguments, it seems likely that the heterogeneity of MOX fuel does enhance fission gas release. Yet, experimental studies on this issue show conflicting results:

- No enhancement effects of the heterogeneous microstructure are reported for MOX fuel operated at low power and low temperature, resulting in low ($\lesssim$3 %) fission gas release fractions (Walker et al., 1996) and (White et al., 2001). In this case, the fission gas release is controlled by athermal processes, which thus seem to be practically insensitive to the heterogeneity of the MOX fuel material. According to White et al. (2001), the athermal fission gas release of MOX is comparable to that of UO_2 fuel, but it starts somewhat earlier in life for the MOX fuel.
- No obvious effects of heterogeneity are reported for MOX fuel operated at high power and temperature, resulting in high ($\gtrsim$30 %) fission gas release fractions[1] (Takahashi et al., 1988). A plausible explanation is that interdiffusion of plutonium and uranium leads to homogenisation of the MOX material at high temperature; see e.g. the works of Billaux and van Vliet (1986), Goll and co-workers (1993), and Ishida and Korei (1994). Moreover, as already mentioned, the enhancing effect of fuel heterogeneity on gas diffusivity decreases with increasing temperature.
- For mixed oxide fuel operated at intermediate power and temperature, data indicate that fission gas release is enhanced in heterogeneous materials (Billaux & van Vliet, 1986) and (Guerin et al., 2000). However, it is not always easy to draw definite conclusions on this issue from comparisons of fission gas release data for various fuel materials, since the microstructures of the compared materials differ not only with respect to the distribution of plutonium. Other characteristics, e.g. grain size, may be equally important.

In conclusion, the data at hand suggest that the MOX fuel heterogeneity affects fission gas release in a certain temperature span: the temperature must be high enough to cause thermal fission gas release, but low enough for the material to maintain its heterogeneous microstructure.

The effect of MOX fuel heterogeneity has been addressed in a few models for fission gas release, which are available in open literature. A common approach in these models is to treat fission gas release from the plutonium-rich agglomerates and the matrix separately, since the two phases of the material differ with respect to isotope composition, fission rate and burnup: the supposedly small difference in temperature is generally neglected.

It is usually assumed that the mechanisms for gas release are identical in agglomerates and matrix, and the same kind of gas release model is used for both phases. Hence, the difference in fission gas release between the phases is attributed entirely to the

[1] This conclusion is based on experience from fast breeder reactor (FBR) rather than LWR fuel.

differences in isotope composition, fission rate and burnup. The total fission gas release from the material is calculated by weighting the contribution from each phase with respect to its volume fraction. This approach is reasonable only in case the two phases are well separated, since it tacitly assumes that i) there is no exchange of fission gas between the phases, ii) the release of gas from phase A is unaffected by the presence of phase B, and vice versa. From post-irradiation examinations of MOX fuel, it is known that part of the fission products created within the plutonium-rich agglomerates migrate into the surrounding matrix (Goll et al., 1993) and (Guerin et al., 2000). Hence, the above assumptions are only partially fulfilled, and the approach may therefore be simplistic in some cases.

The first attempt to model the effect of MOX heterogeneity on fission gas release was made by Billaux and van Vliet (1986). In their model, they neglected fission gas release from the fuel matrix, and considered only the plutonium-rich agglomerates. These were assumed to be spherical, and of uniform size. The isotope composition of the agglomerates, and thus the local fission density and gas production rate, was calculated with respect to time by considering both burnup effects and plutonium/uranium interdiffusion.

More than a decade later, Koo et al. (2000) presented a model based on very much the same concepts as the model by Billaux and van Vliet. However, Koo and co-workers considered fission gas release not only from the agglomerates, but also from the surrounding matrix. To this end, they also proposed a simple method to consider migration of fission fragments from the agglomerates to the matrix. The model originally dealt with agglomerates of uniform size, but it was later extended to treat MOX materials with agglomerates of arbitrary size distributions (Koo et al., 2002). A drawback of the model proposed by Koo et al. is that the change of isotope composition with time, both in the agglomerates and in the fuel matrix, is neglected.

Ishida and Korei (1994) proposed a somewhat different modelling approach. Instead of treating agglomerates and fuel matrix apart, they considered the isotope composition of individual grains in the MOX material. More specifically, they used the statistical frequency distribution for local plutonium concentration, as measured by electron probe microanalysis (EPMA), to define the probability of a grain having a certain concentration of plutonium in the as-fabricated fuel pellet. By calculating the fission gas release on the level of grains for a discrete set of groups, each with a certain as-fabricated plutonium concentration, they determined the average fission gas release from the heterogeneous material. The plutonium concentration of each group was assumed to change with burnup, as a result of fission and capture reactions of plutonium and uranium. Ishida and Korei (1994) applied their model to both LWR and FBR MOX fuel.

In this report, we propose and evaluate a computational model for fission gas release from heterogeneous MOX fuel, which follows the approach by Koo et al. (2000). The proposed model, however, considers the burnup related change of isotope composition in both agglomerates and fuel matrix, in contrast to the original approach by Koo and co-workers. The model is presented in section 2 of the report.

Section 3 deals with calibration and verification of the model against measured data. The irradiation of six instrumented MOX fuel rods is simulated with SKI's version of the FRAPCON-3.3 fuel performance code, in which the proposed fission gas release model has been implemented (Jernkvist, 2008). The calculated fission gas release fractions for these rods are compared with measurements, and the results are discussed in section 4. In addition, section 4 also contains some calculations intended to illustrate the effect of MOX fuel heterogeneity on fission gas release and fuel densification.

2 Model description

The fundamental idea behind the model described in the following subsections is to treat fission gas release from the plutonium-rich agglomerates and the fuel matrix separately, thereby considering the differences in isotope composition, fission rate and burnup between these two phases. The mechanisms for gas release are, however, assumed to be identical for agglomerates and matrix, and a slightly modified form of the GRAGG (Gas Release And Grain Growth) model by Forsberg & Massih (2001, 2007) is applied to calculate the gas release for each phase of the MOX fuel material.[2] Hence, the GRAGG model is used to calculate the fission gas release (FGR) in each phase, based on the appropriate isotope composition, fission rate and burnup. The total gas release from the material is then calculated by weighting the contribution from each phase with respect to its volume fraction.

2.1 Representation of MOX fuel material

In our model, the heterogeneous MOX fuel material is treated by considering two distinct components in the calculations of fission gas release: the fuel matrix and the plutonium-rich agglomerates. Let us assume that the following as-fabricated properties of the material are known:

- Average isotopic composition of the fuel pellet
- Average isotopic composition of the plutonium-rich agglomerates
- Average isotopic composition of the fuel matrix enclosing the agglomerates
- Average, or characteristic, size of the plutonium-rich agglomerates

These are fundamental input data needed for the proposed fission gas release model. Consider now a representative volume element of the material, containing agglomerates enclosed by the fuel matrix. We make the following assumptions regarding the two-component material:

- The Pu-rich agglomerates are of equal size, and treated as spherical particles with radius R_a. Index a will be used to denote properties specific to the agglomerates.
- The fuel matrix enclosing the agglomerates has uniform material properties, fission rate, burnup, etc. Index m will be used to denote matrix-specific properties.

Let v_a and v_m be the volume fractions of agglomerates and matrix material, respectively. Likewise, we denote the weight fraction of plutonia (PuO_2) in the agglomerates and matrix by w_a and w_m. The values of w_a and w_m for the material in un-irradiated, as-fabricated state are known, and the same is true for the fuel average weight fraction of PuO_2, w_h, which can be written

$$w_h = v_a w_a + v_m w_m = w_m + v_a (w_a - w_m), \tag{2.1}$$

[2] The GRAGG model has been referred to as FGRAGG in earlier reports to SKI (Jernkvist, 2005) and (Jernkvist & Massih, 2005).

since $v_a+v_m=1$. Hence, given the weight fractions of PuO_2 in agglomerates, matrix and the fuel pellet material as a whole, the volume fraction of agglomerates follows directly from eq. (2.1)

$$v_a = \frac{w_h - w_m}{w_a - w_m}. \tag{2.2}$$

Although most of the fissions occur in the Pu-rich agglomerates, the fission products do not remain entirely within the agglomerates. Post-irradiation examinations of MOX fuel clearly show that a substantial part of the fission products created within the agglomerates migrates to the surrounding matrix (Walker et al., 1991, Guerin et al., 2000). The migration takes place by direct recoil, knock-on and diffusion of the fission products (Olander, 1976):

- Direct recoil is the migration of energetic fission fragments from a fissioned uranium or plutonium atom. The recoil length, i.e. the length travelled by the fission fragments, is about 10^{-5} m for Xe and Kr in UO_2 and PuO_2 (Matzke, 1982), which means that fission gas atoms created within this distance of the agglomerate surface may be implanted in the matrix by direct recoil.
- Knock-on involves the interaction of a fission fragment or a collision cascade with a stationary atom. The atom that is struck travels about 10^{-8} m in U/Pu oxide fuels. Consequently, only fission product atoms at the very surface of Pu-rich agglomerates can be transferred to the matrix by this mechanism.
- Diffusion of fission products across the interface is possible, but in contrast to direct recoil and knock-on, diffusional transport is largely a thermally activated mechanism. The extent of diffusion thus depends on fuel local temperature and the fission product under consideration.

The transfer of fission products from the Pu-rich agglomerates to the fuel matrix warrants the use of an effective or *equivalent* agglomerate size in the fission gas release model. As shown in figure 2.1, we will henceforth consider a spherical agglomerate with an equivalent radius $R_e=R_a+\lambda$, where λ is a positive model parameter that is less than the typical recoil length of the gaseous fission products Xe and Kr. We assume that the fission rate, burnup, isotope composition and material properties are uniform within the equivalent agglomerate.

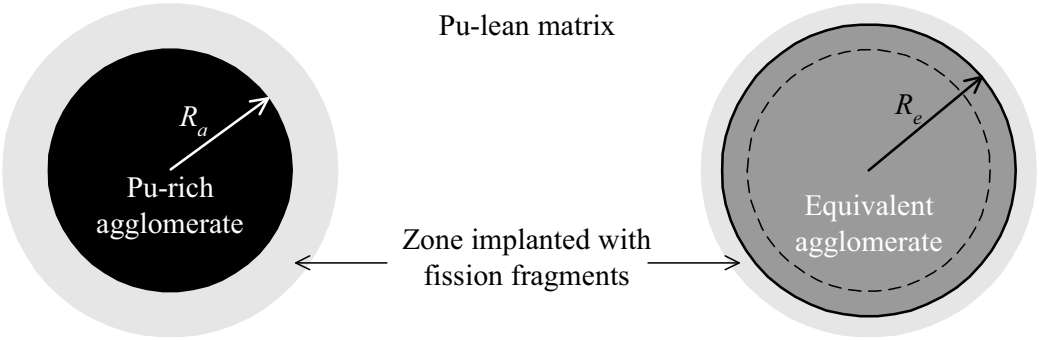

Figure 2.1: Spherical Pu-rich agglomerate with radius R_a, and its equivalent counterpart with radius $R_e=R_a+\lambda$. The equivalent agglomerate, which is assumed to have uniform isotope composition, fission rate and burnup, is used to represent the true agglomerate in calculations of fuel fission gas release.

The concept of equivalent Pu-rich agglomerates with uniform properties in fission gas release modelling is adopted from the works of Koo et al. (2000, 2002). The average plutonia content of the equivalent agglomerate, w_e, is calculated by requiring conservation of mass

$$V_e w_e = V_a w_a + (V_e - V_a) w_m, \tag{2.3}$$

where V_a and V_e are the volumes of the true and equivalent agglomerate, respectively. In the following, we will use index e to denote properties specific to the equivalent agglomerate. By assuming spherical agglomerates, eq. (2.3) leads to

$$w_e = w_m + (w_a - w_m)\left(\frac{R_a}{R_e}\right)^3 = w_m + (w_a - w_m)\left(\frac{R_a}{R_a + \lambda}\right)^3. \tag{2.4}$$

Equation (2.4) is plotted in figure 2.2 for the special case of w_h=0.06, w_m=0.03 and w_a=0.15. It is evident from figure 2.2 that w_e is strongly affected by the choice of λ, and this is particularly true for small agglomerates, i.e. for $R_a \approx \lambda$. In other words, λ is an important model parameter that must be set with care. This issue is not properly discussed in the works of Koo et al. (2000, 2002), where λ is set to 6 µm without further justification.

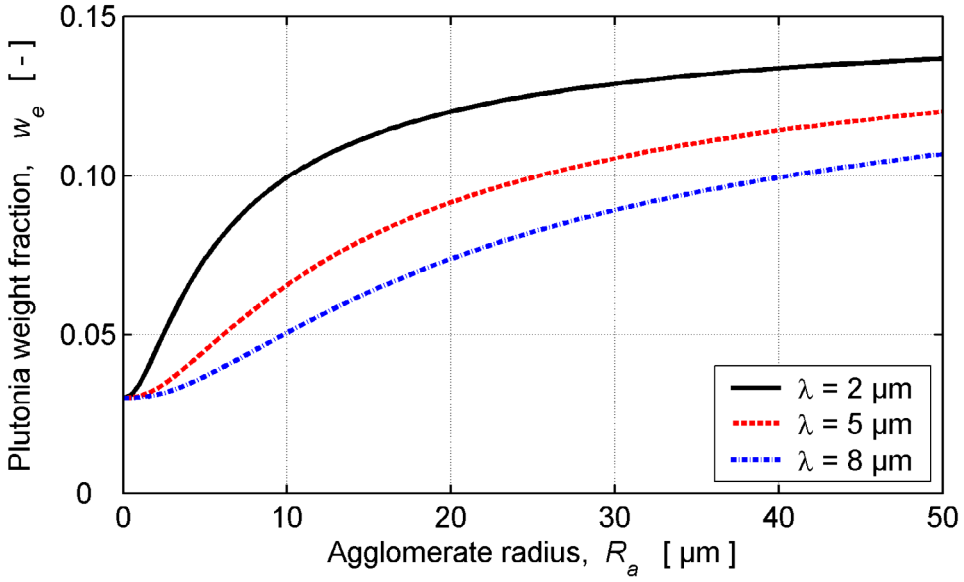

Figure 2.2: Plutonia weight fraction in equivalent agglomerates as a function of true agglomerate radius; see eq. (2.4). In this example, w_h=0.06, w_m=0.03 and w_a=0.15, which are typical as-fabricated values for MIMAS AUC MOX fuel (Garcia et al., 2000).

As mentioned in the introduction, the basic idea behind the proposed model is to treat fission gas release from the fuel matrix and the equivalent agglomerates separately, thereby accounting for the differences in local fission gas rate, isotope composition and burnup between the two components of the heterogeneous fuel material. The fission gas release from the composite material is then calculated by considering the volume fraction of each component.

In similarity with eqs. (2.1) and (2.2), the volume fraction of equivalent agglomerates, v_e, is calculated from

$$v_e = \frac{w_h - w_m}{w_e - w_m}. \tag{2.5}$$

Equation (2.5) is interesting, since it can be used together with eq. (2.4) to determine whether heterogeneity effects are important or not for a specific MOX fuel material. This is illustrated in figure 2.3, which shows v_e as a function of agglomerate radius for the same compositional parameters as used in figure 2.2. Obviously, v_e exceeds unity for small values of R_a. This apparently unphysical result should be interpreted as follows: When $v_e > 1$, the agglomerates are so small that fuel heterogeneity effects on fission gas release are practically insignificant. Gaseous fission products, created within the small agglomerates, are implanted predominantly in the fuel matrix outside the agglomerates, since their transport range is comparable to, or even larger than, the agglomerates. In this case, it is not meaningful to model fission gas release from agglomerates and fuel matrix separately. Whenever v_e exceeds unity, we will therefore treat the material as homogeneous with regard to gas release. From eqs. (2.4) and (2.5), it follows that $v_e>1$ whenever

$$R_a < \lambda \frac{v_a^{1/3}}{1 - v_a^{1/3}}. \tag{2.6}$$

Here, v_a is the agglomerate volume fraction, given by eq. (2.2).

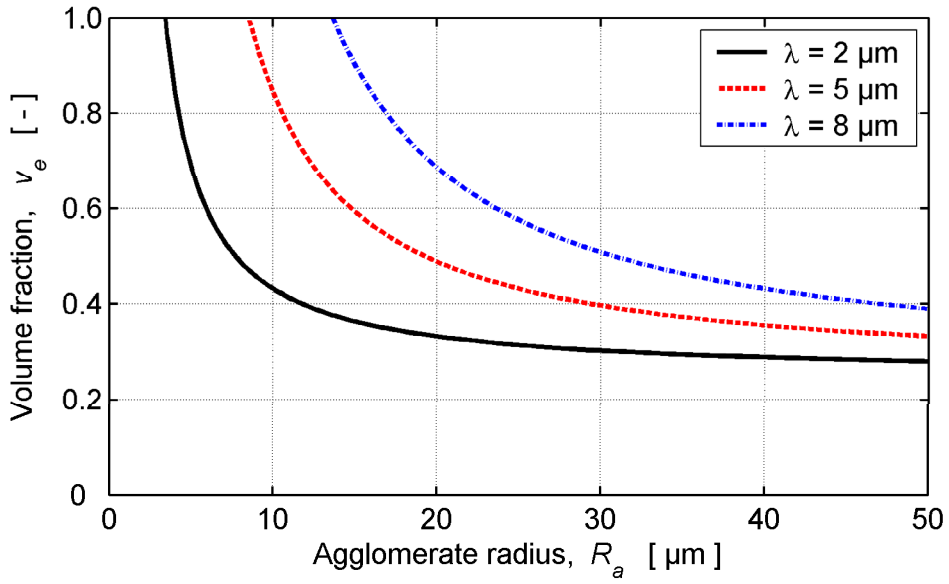

Figure 2.3: Volume fraction of equivalent agglomerates as a function of true agglomerate radius; see eq. (2.5). In this example, w_h=0.06, w_m=0.03 and w_a=0.15, which are typical as-fabricated values for MIMAS AUC MOX fuel (Garcia et al., 2000).

2.2 Calculation of local fission rate and burnup

The local fission rates in the fuel matrix and the equivalent agglomerates are needed to determine the production rate of fission gases in the two components of the heterogeneous material. The local fission rates are also needed to calculate the gas diffusivity and local burnup in the two components.

By assuming that the neutron flux is uniform on a microscopic scale, i.e. the neutron flux in an equivalent agglomerate is identical to the flux in the surrounding fuel matrix, we write the local fission rates in the matrix and equivalent agglomerate as

$$\dot{F}_m = \phi \sum_j \sigma_j^f N_j^m \ , \tag{2.7}$$

$$\dot{F}_e = \phi \sum_j \sigma_j^f N_j^e \ . \tag{2.8}$$

Here, $\dot{F}$ is the fission rate [fissions/(m^{3}s)], ϕ is the total neutron flux [neutrons/(m^{2}s)], N_j is the number density [atoms/m^3] of fissile isotope *j* in the material, and σ_j^f is the effective, one-group, microscopic cross section [m^2/atom] for fissioning of isotope *j*. As before, *m* and *e* indicate properties of the fuel matrix and the equivalent agglomerates, respectively.

The local fission rate calculated by the TUBRNP submodel (Lassmann et al., 1994) in the FRAPCON computer code is related to a material in which matrix and agglomerates are homogenized. Denoting this fission rate by $\dot{F}_h$, we formally write

$$\dot{F}_h = \phi \sum_j \sigma_j^f N_j^h \ , \tag{2.9}$$

where N_j^h is the number density of isotope *j* in the homogenized material. Our intention is to make use of the existing TUBRNP model for local fission rate calculations, and we therefore define two enhancement factors, p_m and p_e, by which the fission rate in the homogeneous material should be multiplied to obtain the fission rates in the fuel matrix and the equivalent agglomerates, respectively. By combining eqs. (2.7)-(2.9), these enhancement factors can be written

$$p_m = \frac{\dot{F}_m}{\dot{F}_h} = \sum_j \sigma_j^f N_j^m \Big/ \sum_j \sigma_j^f N_j^h \ , \tag{2.10}$$

$$p_e = \frac{\dot{F}_e}{\dot{F}_h} = \sum_j \sigma_j^f N_j^e \Big/ \sum_j \sigma_j^f N_j^h \ . \tag{2.11}$$

In our model, we will consider the fissile isotopes ^{235}U, ^{238}U, ^{239}Pu, ^{240}Pu, ^{241}Pu and ^{242}Pu. The cross sections for fissioning of these isotopes, applied in our model, are listed in table 2.1.

Isotope ^{j}X	σ_j^f [10^{-28} m^2]	σ_j^c [10^{-28} m^2]
^{235}U	41.5	9.7
^{238}U	0.0	0.78
^{239}Pu	105.0	58.6
^{240}Pu	0.584	100.0
^{241}Pu	120.0	50.0
^{242}Pu	0.458	80.0

Table 2.1: One-group cross sections for fission, σ_j^f, and neutron capture, σ_j^c, of the considered uranium and plutonium isotopes. The cross sections are taken from the TUBRNP model by Lassmann et al. (1994), and pertain to typical light water reactor neutron energy spectra.

The cross sections in table 2.1 are one-group effective cross sections, meaning that they are averaged over the energy spectrum of the neutron flux, i.e.

$$\sigma = \int_0^\infty \sigma'(E)\,\phi(E)\,dE \Big/ \int_0^\infty \phi(E)\,dE\,, \tag{2.12}$$

where E is the neutron energy. The one-group cross sections in table 2.1 are taken from the work of Lassmann et al. (1994), and pertain to typical energy spectra of the neutron flux in BWRs and PWRs.

The fission rate enhancement factor for equivalent agglomerates, given by eq. (2.11), is illustrated in figure 2.4 for typical MIMAS AUC (Micronised Masterblend Ammonium Uranyl-plutonyl Carbonate) MOX fuel in un-irradiated state. The typical as-fabricated isotope composition of this kind of fuel is given in table 2.2. As expected, the fission rate enhancement factor increases with agglomerate size, but there is also a strong dependence on the extrapolation length λ. We note that $p_e < 1$ for R_a satisfying the condition in eq. (2.6). As before, we conclude that the heterogeneous material model should not be applied in this region.

Equations (2.10) and (2.11) provide a more rigorous definition of the fission rate enhancement factors than the ones used in earlier models for fission gas release in heterogeneous MOX fuel. For instance, Ishida & Korei (1994) introduced a fixed ratio, $\kappa = \sigma_U^f / \sigma_{Pu}^f$, and defined the fission rate enhancement factor as

$$p_m = \frac{\dot{F}_m}{\dot{F}_h} \approx \frac{w_m + \kappa(1 - w_m)}{w_h + \kappa(1 - w_h)}, \tag{2.13}$$

$$p_e = \frac{\dot{F}_e}{\dot{F}_h} \approx \frac{w_e + \kappa(1 - w_e)}{w_h + \kappa(1 - w_h)}, \tag{2.14}$$

where w_m, w_e and w_h are the plutonia weight fractions in the fuel matrix, the equivalent agglomerates and the homogenized material, respectively.

Koo and co-workers (2000, 2002) took this simplification one step further in their model and neglected the fissioning of uranium completely. Hence, they set $\kappa = 0$, and defined the fission rate enhancement factors as $p_m = w_m / w_h$ and $p_e = w_e / w_h$.

Another important point to make is that Koo and co-workers (2000,2002) considered a constant (time-independent) composition of the fuel material. Hence, they assumed that the fission rate enhancement factors do not change with fuel burnup. Ishida and Korei (1994), on the other hand, considered that w_h, w_m and w_e depend on burnup, and treated p_m and p_e as time-varying parameters. This approach will be followed also in our model, by calculating the changes to the isotope composition of fuel matrix and equivalent agglomerates under irradiation.

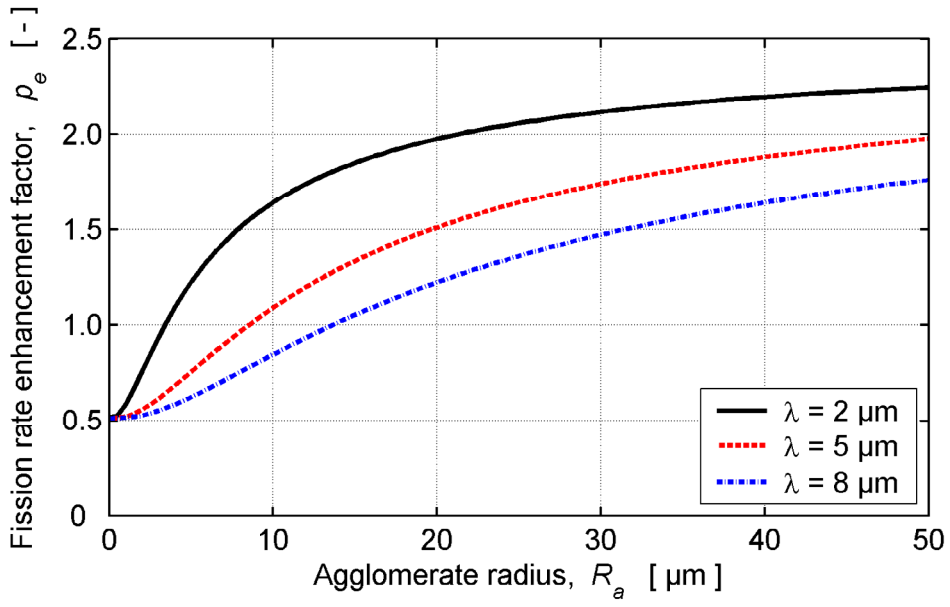

Figure 2.4: Fission rate enhancement factor in equivalent agglomerates as a function of true agglomerate radius; see eq. (2.11). In this example, w_h=0.06, w_m=0.03 and w_a=0.15, which are typical as-fabricated values for MIMAS AUC MOX fuel (Garcia et al., 2000). The isotope composition of the fuel is given in table 2.2.

Isotope composition (atomic%)	
Uranium	Plutonium
^{235}U / ^{Tot}U = 0.25 ^{238}U / ^{Tot}U = 99.75	^{239}Pu / ^{Tot}Pu = 65 ^{240}Pu / ^{Tot}Pu = 24 ^{241}Pu / ^{Tot}Pu = 7 ^{242}Pu / ^{Tot}Pu = 4

Table 2.2: Typical isotope composition of MIMAS AUC MOX fuel (White, 1999) and (Koike, 2004).

2.3 Calculation of local fuel composition

The relations derived in the preceding subsection contain the isotope composition of the fuel matrix and the equivalent agglomerates as fundamental parameters. The initial isotope compositions of these components are provided as fuel design input to the calculations, but as the fuel is burnt, the isotope compositions change. These changes may be neglected in analyses of low-burnup fuel, but as will be shown below, they have to be considered for fuel with medium to high burnup.

Changes to the fuel isotope composition are in our model calculated by use of burnup equations adopted from the TUBRNP model by Lassmann et al. (1994). Separate sets of equations are used for the fuel matrix and the equivalent agglomerates, but the formulation of the equations is identical for both components of the material. A third set of equations is used to calculate the isotope composition of the homogenized fuel material; this corresponds to the original implementation of the model in FRAPCON.

The burnup equations are (Lassmann et al., 1994)

$$\frac{dN^k_{235}(\bar{r})}{dt} = -\phi(\bar{r})\, N^k_{235}(\bar{r})\, \sigma^a_{235}, \tag{2.15}$$

$$\frac{dN^k_{238}(\bar{r})}{dt} = -\phi(\bar{r})\, \overline{N}^k_{238}(z)\, \sigma^a_{238}\, f(r), \tag{2.16}$$

$$\frac{dN^k_{239}(\bar{r})}{dt} = -\phi(\bar{r})\left[\, N^k_{239}(\bar{r})\, \sigma^a_{239} - \overline{N}^k_{238}(z)\, \sigma^c_{238}\, f(r) \,\right], \tag{2.17}$$

$$\frac{dN^k_j(\bar{r})}{dt} = -\phi(\bar{r})\left[\, N^k_j(\bar{r})\, \sigma^a_j - N^k_{j-1}(\bar{r})\, \sigma^c_{j-1} \,\right]. \tag{2.18}$$

Here, j=240,241,242 refers to the plutonium isotopes, N^k_j is the number density of each fissionable isotope j in material k, where k alludes to the fuel matrix (k=m), the equivalent matrix (k=e), or the homogenized material (k=h). The neutron flux depends on the position, $\bar{r}$, in the fuel pellet column, and so does the number densities of the considered isotopes. The quantity $\overline{N}^k_{238}(z)$ in eqs. (2.16) and (2.17) is the radial average concentration of ^{238}U at axial position z.

In eqs. (2.15)-(2.18), σ^a_j and σ^c_j are microscopic cross sections for neutron absorption and neutron capture, respectively. The absorption cross section is the sum of the cross sections for fission and capture. As before, the applied cross sections are averaged over the neutron energy spectrum, and with the exception of σ^c_{238}, they are assumed to be constant across the fuel pellet radius. The radial dependence of σ^c_{238} is due to the fact that resonance capture of epithermal neutrons by ^{238}U is strongly peaked to the pellet surface (Stacey, 2001). This effect is considered by the radial shape function $f(r)$ in eqs. (2.16) and (2.17). This is an empirical function, given by Lassmann et al. (1994) as

$$f(r) = C_0\left(1 + 3.45\, e^{-3(R_{po}-r)^{0.45}}\right), \tag{2.19}$$

where r is the radial position, R_{po} is the pellet outer radius and C_o is a normalization constant, such that

$$2 \int_{R_{pi}}^{R_{po}} f(r)\, r\, dr \Big/ \left(R_{po}^2 - R_{pi}^2 \right) = 1. \qquad (2.20)$$

Here, R_{pi} is the pellet inner radius; R_{pi}=0 for solid (non-annular) fuel pellets. The empirical shape function in eq. (2.19) is valid for typical neutron energy spectra in BWRs and PWRs, but not for other reactor types. Also the cross sections are specific to light water reactors; see table 2.1. However, it should be remarked that a similar burnup model has been presented for heavy water reactors (Lassmann et al., 1998).

As already mentioned, eqs. (2.15)-(2.18) are solved for the fuel matrix, the equivalent agglomerates and the homogenized material separately, based on a common neutron flux distribution, $\phi(\bar{r})$. A simple explicit Euler time stepping scheme is used for the numerical solution. The flux is given by the prescribed linear heat generation rate and the distribution of fissile isotopes in the homogenized material (Lassmann et al., 1994). The results of the calculations, i.e. the isotope number densities N_j^k, define the fission rate enhancement factors p_m and p_e through eqs. (2.10) and (2.11). Accordingly, the enhancement factors change with fuel burnup. This is illustrated in figures 2.5 and 2.6, which show the burnup dependence of p_m and p_e for a typical PWR fuel rod, charged with MIMAS AUC MOX fuel. The considered rod is from a 17×17 fuel assembly, and the fuel pellet diameter is 8.19 mm. The isotope composition of the considered fuel is given in table 2.2, and as before, the as-fabricated weight fractions of plutonia were w_h=0.06, w_m=0.03 and w_a=0.15. In the calculations, it was assumed that R_a=25 μm and λ=5 μm, and fifty radial nodes were used to discretize the fuel pellet.

Figure 2.5 shows the calculated fission rate enhancement factors at the pellet centre, whereas figure 2.6 pertains to the pellet periphery. It is clear that the fission rate enhancement decreases with increasing burnup, and that the rate of decrease is faster at the pellet periphery than at the pellet centre. This results from the higher fission rate at the pellet periphery, which leads to a faster consumption of fissile isotopes in the fuel. From figure 2.6, we note that the fission rate at the pellet periphery actually gets higher in the fuel matrix than in the equivalent agglomerates, beyond a pellet radial average burnup of about 48 MWd(kgHM)$^{-1}$; this corresponds to a local burnup of 70 MWd(kgHM)$^{-1}$ at the pellet rim. At this burnup and beyond, most fissile isotopes in the original, as-fabricated, material have been burnt, and the fission rate is largely controlled by neutron capture of ^{238}U, leading to formation and fissioning of ^{239}Pu. Since the as-fabricated concentration of ^{238}U is 7.6 % higher in the matrix than in the equivalent agglomerates, the calculated fission rate at end of life tends to be 7.6 % higher in the matrix than in the agglomerates, as shown in figure 2.6.

Finally, the plutonia weight fraction, w_k, is calculated through

$$w_k = \sum_{j=239}^{242} j N_j^k \Big/ \left(\sum_{j=239}^{242} j N_j^k + 235 N_{235}^k + 238 N_{238}^k \right), \qquad (2.21)$$

where k is either m (matrix), e (equivalent agglomerates) or h (homogenized material).

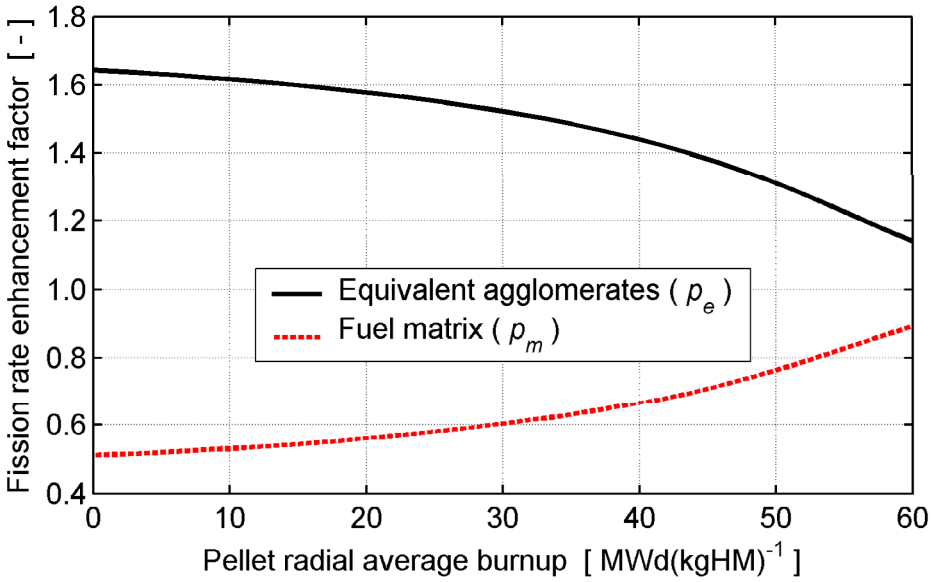

Figure 2.5: Fission rate enhancement factors at the pellet centre (r=0) calculated for typical MIMAS AUC MOX fuel with R_a=25 µm and λ=5 µm. For this example, the end-of-life pellet radial average burnup of 60 MWd(kgHM)$^{-1}$ corresponds to a local burnup of about 56 MWd(kgHM)$^{-1}$ at the pellet centre.

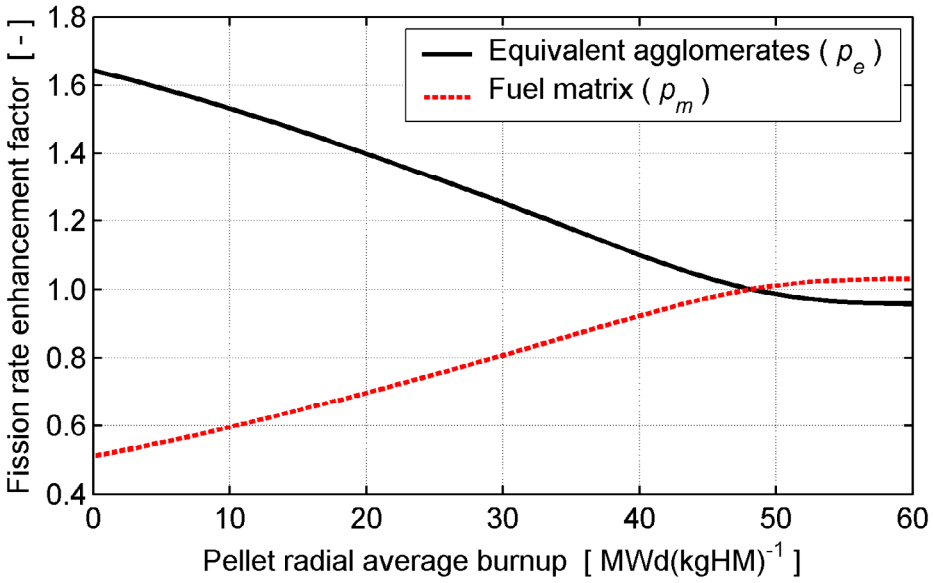

Figure 2.6: Fission rate enhancement factors at the pellet periphery (r=R_{po}) calculated for typical MIMAS AUC MOX fuel with R_a=25 µm and λ=5 µm. For this example, the end-of-life pellet radial average burnup of 60 MWd(kgHM)$^{-1}$ corresponds to a local burnup of about 97 MWd(kgHM)$^{-1}$ at the pellet periphery.

2.4 Calculation of fission gas release

Following the calculations of fission rate enhancement factors, burnup and isotope composition for the equivalent agglomerates and the fuel matrix, these data are used to calculate the production and release of fission gases for each component of the MOX material. The GRAGG (Gas Release And Grain Growth) model by Forsberg & Massih (2001, 2007) is used for this purpose. The fundamentals of this model are described in an earlier report (Jernkvist & Massih, 2005), where also sample calculations are presented to illustrate important features of the model.

The GRAGG model was recently implemented in SKI's version of the FRAPCON-3.3 computer code, and calibrated against a fairly extensive database on fission gas release from uranium dioxide fuel (Jernkvist, 2005). A similar calibration must be done against data for mixed oxide fuel, and this calibration is the topic of section 3.

Mixed oxide fuels with homogeneous distributions of plutonium, i.e. fuels with as-fabricated microstructures satisfying eq. (2.6), are treated as homogeneous continua. For such materials, GRAGG is called with the average (homogeneous) material properties as input, and the fission gas release is calculated in the same manner as for UO_2 fuel, but with slightly different model parameters; see section 3.3.

If the MOX material is heterogeneous, i.e. if eq. (2.6) is not satisfied, GRAGG is called twice: one call is made for the equivalent agglomerates and another one for the fuel matrix, using in each call the appropriate fission rate and burnup for the considered component of the material. The fractional gas release in the i:th nodal point of the discretized fuel pellet column, $\Re^i$, is then calculated from

$$\Re^i = \frac{v_e R_e^i + (1-v_e) R_m^i}{v_e P_e^i + (1-v_e) P_m^i} , \tag{2.22}$$

where R_e^i and R_m^i are the calculated amounts of gas [mol/m^3] released in node i from the equivalent agglomerates and the matrix, respectively, and P_e^i and P_m^i are the corresponding amounts of gas produced in the two components of the material.

The procedure is applied to each nodal point, using local (nodal) values for fuel temperature and homogenized fission density ($\dot{F}_h$) in the calculations. The rod average release fraction, $\Re$, is simply calculated by summing the amount of released gas and dividing it by the total gas production

$$\Re = \frac{\sum_{i=1}^{N} \left[v_e R_e^i + (1-v_e) R_m^i \right] V^i}{\sum_{i=1}^{N} \left[v_e P_e^i + (1-v_e) P_m^i \right] V^i} . \tag{2.23}$$

Here, N is the number of nodes in the discretized fuel pellet column, and V^i is the volume [m^3] of the i:th node. The number of nodes to be used in a calculation is set as user defined input to FRAPCON-3.3.

The gaseous fission products considered by the GRAGG model are xenon and krypton. A separate model in FRAPCON-3.3 treats production and release of helium. The helium release model, which is described in the program documentation (Lanning et al., 2005), has not been changed in the work presented here.

The fission gas produced in MOX fuel has a different composition than gas produced in UO_2. The fissile content of MOX fuel mainly consists of the plutonium isotopes ^{239}Pu and ^{241}Pu, which have a higher fission yield of xenon but a lower yield of krypton than ^{235}U (White, 2000). Accordingly, the ratio of xenon to krypton is much higher for fission gas produced in MOX than in UO_2 fuel. Since the fission gas composition may influence pellet-to-cladding heat transfer in cases where excessive gas release occurs, the difference in gas composition between MOX and UO_2 fuel is accounted for in FRAPCON-3.3. The code uses a Xe/Kr ratio of 5.67 for fission gas produced in UO_2 fuel, and a Xe/Kr ratio of 16.0 for MOX fuel (Lanning et al., 2005). These values are used irrespective of the fuel isotope composition. A more accurate approach would be to calculate the Xe/Kr ratio of the produced gas based on the true isotope composition, considering its burnup dependence. This approach was tested in an earlier project for SKI (Jernkvist & Massih, 2002).

It should be remarked that re-structuring of plutonium-rich agglomerates at high burnup is not yet properly accounted for in the proposed fission gas release model. Although a pellet re-structuring model is included in SKI's version of FRAPCON-3.3, it currently treats the MOX fuel as homogeneous. The model, which is described in section 2.1 of (Jernkvist & Massih, 2005), therefore needs modification to consider agglomerates and fuel matrix separately.

3 Calibration and verification of the model

Some parameters in the proposed model have been calibrated against fission gas release data for mixed oxide fuel. The calibration was aimed to obtain best possible agreement between measured data and fission gas release fractions calculated with SKI's version of FRAPCON-3.3, into which the proposed model has been implemented (Jernkvist, 2008). The calibration is described below, and the optimised model parameters are presented. To this end, it should be mentioned that the GRAGG model implementation in FRAPCON-3.3 has been verified and validated against fission gas release data for UO_2 fuel in an earlier project for SKI (Jernkvist, 2005).

3.1 Database used for model calibration

An integral assessment and calibration of the FRAPCON computer code has been done by the code developers at the Pacific Northwest National Laboratory (PNNL). The assessment was done by comparing the calculated fuel temperature, fission gas release, clad deformation and clad oxide layer thickness with post-irradiation measurements for a number of LWR fuel rods. Models in the code were thereby calibrated on a best-estimate basis.

The database used by PNNL for integral assessment and calibration comprised about 40 UO_2 fuel rods (Lanning et al.,1997b) and 6 MOX fuel rods (Lanning et al., 2005). The assessment database for the UO_2 fuel rods is made available to the FRAPCON user community by PNNL, not only by supplying the test data, but also by providing input files for all assessment cases. However, this is not the case for their MOX fuel database, and calibration of the MOX fuel fission gas release model was therefore done against a database, which was compiled from literature sources independently of PNNL. Yet, our MOX fuel database comprises some experiments that have also been used for model calibration by PNNL (Lanning et al., 2005). The FRAPCON-3.3 input files for our assessment cases were constructed from various literature sources, as defined in appendix A. Since all fuel rod power histories were extracted from graphs and plots in these sources, there are some uncertainties connected with the simulated irradiation histories. The same is true for reactor coolant conditions and axial power distributions.

Key data for the six MOX fuel rods used in our calibration of the fission gas release model are summarized in table 3.1, and details are given in appendix A. The rods, or rodlets, were irradiated in four different instrumented fuel assemblies (IFAs) in the Halden reactor. Four of the rodlets were re-fabricated (sampled) from full-length PWR fuel rods, which had been irradiated to high burnup in power generating reactors. The fission gas release during the pre-irradiation phase, as given in the rightmost column of table 3.1, was estimated from the measured fission gas release of the full-length mother rods upon re-fabrication. All the considered test rods were of PWR design, and charged with MOX fuel fabricated through the MIMAS process.

Experiment, fuel rod	Fuel rod design	Base irradiation	Burnup [MWd(kgHM)$^{-1}$]	Peak LHGR [kWm^{-1}]	R_a [µm]	S_o [µm]	EOL FGR [%]	Base FGR [%]
IFA-597, rod 10 IFA-597, rod 11	PWR 17×17	Halden, Norway	37-38	36	7.6	5.5	16 13	- -
IFA-606, rod sg IFA-606, rod lg	PWR 14×14	Beznau 1, Switzerland	45-47	33	8.0	8.0 11.0	15 15	2 2
IFA-629.1, rod 2	PWR 17×17	St Laurent B1, France	41	37	3.5	11.7	22	0
IFA-629.3, rod 6	PWR 17×17	Graveline 4, France	60	24	8.3	6.8	12	4

Table 3.1: Summary of Halden reactor experiments on MOX fuel rodlets used for assessment and calibration of the fission gas release model.

Peak LHGR: Peak value of rodlet average linear heat generation rate.
R_a: As-fabricated average radius of plutonium-rich agglomerates.
S_o: As-fabricated average grain size.
EOL FGR: Measured end-of-life fission gas release (rodlet average) in percent of produced gas.
Base FGR: Fission gas release (rodlet average) under base irradiation, estimated from measured FGR of full-length mother rod.

The six fuel rods in table 3.1 were selected for model calibration, since in all rods, the fission gas release was measured as a function of time by use of internal pressure transducers.[3] Data in the form of fission gas release versus time are more valuable for model calibration than just end-of-life fission gas release measurements, as will be discussed in the following subsection.

3.2 Calibration method

A few parameters in the proposed fission gas release model were tuned to obtain the best possible agreement between calculated fission gas release and the database. The "best possible agreement" was sought by minimizing the L2-norm of relative errors, defined by

$$\Gamma = \sqrt{\sum_{j=1}^{M} \left(\frac{\Re_c^j - \Re_m^j}{\Re_m^j} \right)^2} , \qquad (3.1)$$

where $\Re_c^j$ and $\Re_m^j$ are the calculated and measured gas release fractions for case j, and M is the number of comparisons between calculated and measured release fractions. In our calibration, M=14, which means that the number of comparisons is larger than the number of fuel rods in the database: since the fission gas release was measured as a function of time, it was possible to compare the calculated and measured release fractions not only at end-of-life, but also at other points in time.

By searching for an optimum with respect to relative rather than absolute errors, emphasis was placed on model accuracy for cases with low fission gas release, i.e. for cases that are most relevant to normal operating conditions. The minimization of Γ was performed by full search, i.e. by calculating Γ for all conceivable combinations of the model parameters to be optimised. The same computational mesh was used in all calculations with FRAPCON-3.3: all rodlets were discretized into 4 axial segments, and 45 radial nodes were used to represent the fuel pellet column in each of these segments.

3.3 Optimised model parameters

The GRAGG model in SKI's version of FRAPCON-3.3 has earlier been calibrated against fission gas release data for UO_2 fuel (Jernkvist, 2005), and most of the model parameters set in that calibration are expected to work also for mixed oxide fuel. Hence, the parameters considered for calibration in the present work are either specific to the MOX fuel fission gas release model, or expected to differ between MOX and UO_2 fuel.

The following parameters in the MOX fuel fission gas release model were optimised:

- The extrapolation length, λ, of the agglomerate radius. From section 2.1, it is clear that λ is a key parameter for describing the MOX fuel heterogeneity.

[3] Data for fission gas release versus time for the two IFA-606 test rods are, however, unavailable in open literature.

- The fission gas diffusivity, D, in the fuel material. The diffusivity of xenon and krypton could possibly be different in MOX than in pure UO_2 fuel. However, there are no data to either support or refute this suspicion.
- The gas concentration at grain boundaries, N_{sat}, at which the grain boundary is saturated and part of the gas at the grain face is released to the rod free volume through a network of interconnected intergranular bubbles. Post irradiation studies suggest that grain boundary fission gas behave differently in $(Pu,U)O_2$ than in UO_2 fuel, presumably as a result of enhanced grain boundary diffusivity (Guerin et al., 2000). It is therefore likely that N_{sat} differs between MOX and UO_2 fuel.

The optimised values of these parameters are presented and discussed in the sequel. It should be remarked that the optimised parameters for D and N_{sat} in mixed oxide fuel have been implemented as MOX-specific material property correlations in the FRAPCON-3.3 GRAGG model, and different correlations are thus used for UO_2 and MOX fuel materials.

3.3.1 Extrapolated agglomerate radius

The plutonium-rich agglomerates in the MOX fuel material are in the proposed model represented by equivalent agglomerates of spherical form and uniform size. Migration of fission fragments from the agglomerates to the surrounding matrix is considered in the definition of the equivalent agglomerate radius through the extrapolation length, λ. As discussed in section 2.1, λ should be less than the typical recoil length of the fission fragments Xe and Kr in UO_2 and PuO_2. The optimum value obtained for λ in our calibration is 2.55 μm. This value should be considered tentative, since most fuel rods in the considered database are charged with MOX fuel with similar microstructure and therefore provide very little information on fuel heterogeneity effects. From table 3.1, it is clear that all rods except for one have practically the same average agglomerate size.

3.3.2 Fission gas diffusivity

The GRAGG model considers Xe and Kr gas atoms, which diffuse from the interior of fuel grains to the grain boundaries. The diffusivity, D, of these fission gas species within the fuel grains is in the model calculated through

$$D = D_{\text{int}} \Omega_g , \tag{3.2}$$

where D_{int} [m^2s^{-1}] is the intrinsic diffusivity of a trap-free material, i.e. a material without intragranular bubbles, and Ω_g is dimension-free reduction factor that accounts for gas trapping in intragranular bubbles. The latter depends on temperature, fission density and time (Jernkvist, 2005) and (Jernkvist & Massih, 2005).

The intrinsic diffusivity in eq. (3.2) is correlated to fuel temperature T [K] and fission density $\dot{F}$ [fissions$(m^3s)^{-1}$] through a model, which is based on the experimental work of Turnbull et al. (1982)

$$D_{\text{int}} = C_1 e^{-Q_1/T} + C_2 \sqrt{\dot{F}}\, e^{-Q_2/T} + C_3 \dot{F} . \tag{3.3}$$

Turnbull and co-workers determined the constant model parameters Q_1, Q_2, C_1, C_2 and C_3 based on in-reactor experiments on Xe and Kr release from UO_2 over the temperature range 520-1670 K. To the author's best knowledge, no corresponding

experiment exists for MOX fuel. The first and last term on the right-hand-side of eq. (3.3) pertain to thermal and athermal contributions, respectively, to the gas diffusivity. The second term represents a mixed contribution, and this term generally dominates the total in-reactor diffusivity over the temperature range of 1100 to 1800 K; see the work of Turnbull et al. (1982).

To identify possible differences in intrinsic gas diffusivity between MOX and UO_2 fuel, C_1, C_2 and C_3 of eq. (3.3) were included in the model calibration. The optimum values for these coefficients, both for MOX and UO_2 fuel, are presented in table 3.2 together with the original values reported for UO_2 fuel by Turnbull et al (1982). The values for Q_1 and Q_2, 35247 and 13800 K, respectively, were not altered.

From table 3.2, it is clear that the optimum values for C_1 and C_3 are about 10 % lower for MOX than for UO_2 fuel. The difference in fission gas diffusivity between the materials thus seems to be almost negligible at low and very high temperature. In contrast, the optimum value for C_2 differs considerably between the materials, which would suggest a non-negligible difference in gas diffusivity between MOX and UO_2 fuel for temperatures between 1100 and 1800 K. However, the difference can also be a consequence of improper consideration of the confining role of the fuel matrix upon gas release in our model. This is discussed in section 4.4.

Coefficient in equation (3.3)	**Turnbull et al. (1982)**	**Optimised values**	
		MOX	**UO_2**
C_1 [m^2s^{-1}]	7.60×10^{-10}	1.17×10^{-9}	1.30×10^{-9}
C_2 [$m^{7/2}s^{-1/2}$]	1.70×10^{-25}	1.62×10^{-25}	7.70×10^{-25}
C_3 [m^5]	2.00×10^{-40}	1.23×10^{-39}	1.37×10^{-39}

Table 3.2: Optimum values for coefficients in the expression for intrinsic gas diffusivity in comparison with the experimental results reported by Turnbull et al. (1982). The optimised values for UO_2 fuel were determined in an earlier project (Jernkvist, 2005).

3.3.3 Grain boundary gas saturation threshold

The gas atoms diffuse to the grain boundaries, where they are trapped in intergranular bubbles. Eventually, the grain boundaries are saturated with gas, meaning that the bubbles coalesce and form an interconnected network, through which gas is vented to the rod free volume. If the ideal gas equation of state is assumed, the surface concentration of intergranular gas at saturation, N_{sat} [mol/m^2], can be calculated through

$$N_{sat} = \frac{4 r_f f(\theta) f_b}{3 k_B T \sin^2\theta} \left(\frac{2\gamma}{r_f} + P_{hyd} \right), \tag{3.4}$$

where $f(\theta) = 1 - 1.5\cos\theta + 0.5\cos^3\theta$ is a shape factor, θ the dihedral angle between the bubble surface and the grain boundary, k_B the Boltzmann constant, T [K] the fuel temperature, r_f [m] the projected radius of the curvature of the capillary surface of the bubble, and γ [Nm^{-1}] its surface tension.

Moreover, f_b is the grain boundary fraction covered with bubbles upon saturation, and P_{hyd} [Pa] is the hydrostatic pressure within the fuel. In the FRAPCON-3.3 implementation of the GRAGG model, P_{hyd} is taken as the sum of the rod internal gas pressure and the pellet-clad contact pressure.

Since there is considerable uncertainty in many of the parameters in eq. (3.4), the expression for N_{sat} was calibrated to experimental data. In the calibration, the functional form for N_{sat} with respect to temperature and hydrostatic pressure was retained in keeping with eq. (3.4), and only the coefficients were tuned. Hence, the resulting optimised expression for N_{sat} is

$$N_{sat} = \frac{C_4}{T}\left(2.4\times10^{6} + P_{hyd}\right) \tag{3.5}$$

where the value of C_4 was found to be slightly different for MOX than for UO_2 fuel. C_4=8.12×10^{-9} molKN^{-1} is the optimum value for MOX, obtained from calibration to the database in appendix A. This is 25 % higher than the optimum value obtained for UO_2 fuel (6.50×10^{-9}) in an earlier work (Jernkvist, 2005). Considering the rather limited database from which these values are derived, it is questionable whether this difference in C_4 between MOX and UO_2 would suggest any significant difference in grain boundary gas saturation threshold between the two materials.

4 Results and discussion

4.1 Comparison of FRAPCON-3.3 fission gas release models

Table 4.1 presents calculated and measured fission gas release fractions for the six MOX fuel rods that were used for model assessment and calibration. As explained in section 3.2, data on fission gas release versus time are available for four of the rods, and comparisons between measured data and calculated gas release are made at several points in time for these rods, as shown in table 4.1.

The calculations were done with two different models for MOX fuel fission gas release in SKI's version of FRAPCON-3.3:

- The MASSIH model by PNNL (Lanning et al., 1997a) and (Lanning et al., 2005). This model treats fission gas release of UO_2 fuel and MOX fuel alike, but the fission gas diffusivity is increased by a factor 1.75 for MOX relative to UO_2 fuel.
- The proposed model, henceforth called MOX GRAGG. The optimised model parameters from section 3.3 are used in the calculations.

In the rightmost column of table 4.1, results are also shown for the special case of assuming a homogeneous distribution of plutonium in calculations with the MOX GRAGG model ("HOMOGENEOUS"). Assuming homogeneity is done by setting the agglomerate radius R_a to a small value, typically < 1 μm, in input to the model. These calculations were done to illustrate the effect of plutonium distribution in the considered fuel rods.

The L2-norm of relative differences between calculated and measured fission gas release, i.e. Γ from eq. (3.1), is shown for each of the models at the bottom of table 4.1. The comparison between calculated and measured fission gas release in table 4.1 is also shown graphically in figure 4.1.

The closest agreement between measured and calculated results is reached with the MOX GRAGG model. From table 4.1, it is clear that Γ obtained with this model is less than half of that reached with the PNNL MASSIH model. From figure 4.1, it is obvious that the PNNL MASSIH model has a tendency to overestimate the fission gas release for the considered cases.

The MOX GRAGG model gives reasonable results, but there are three data points for which the fission gas release is significantly underestimated. These points pertain to rod 2 in IFA-629.1. As explained in section A.3 of appendix A, this rod was characterized by an unusually homogeneous distribution of plutonium, and it was operated at high power, up to 37 kWm^{-1}, during the end-of-life irradiation period in Halden. Further analyses are needed to identify why the MOX GRAGG model fails to accurately capture the fission gas release for this particular case.

Halden IFA and test rodlet	Burnup [MWd/ (kgHM)]	Measured FGR [%]	Calculated FGR [%]		
			PNNL MASSIH	MOX GRAGG	HOMO-GENEOUS
IFA-597 rod 10	16.9	6.5	12.8	8.3	8.3
	37.2	16.0	20.3	16.0	16.0
IFA-597 rod 11	17.6	9.5	10.9	6.2	6.2
	38.0	13.0	16.3	14.3	14.3
IFA-606 rod sg	45.2	15.0	25.9	14.2	11.8
IFA-606 rod lg	47.0	15.0	28.3	15.8	11.7
IFA-629.1 rod 2	30.2	3.0	8.0	3.4	3.4
	30.4	9.0	15.5	4.5	4.5
	31.3	18.5	26.6	8.8	8.8
	40.8	22.0	29.8	15.4	15.4
IFA-629.3 rod 6	59.1	3.9	5.8	5.0	0.9
	59.3	8.1	11.5	8.3	2.8
	59.5	10.8	12.3	8.7	3.1
	59.6	11.6	12.3	9.3	3.3
L2-norm of errors, Γ			**2.540**	**1.0017**	**1.7247**

Table 4.1: Comparison of models for MOX fuel fission gas release, available in SKI's version of FRAPCON-3.3. The measurements pertain to the assessment database in appendix A. Γ is the goodness of fit, defined by the L2-norm of relative differences between calculated and measured fission gas release fractions; see eq. (3.1).

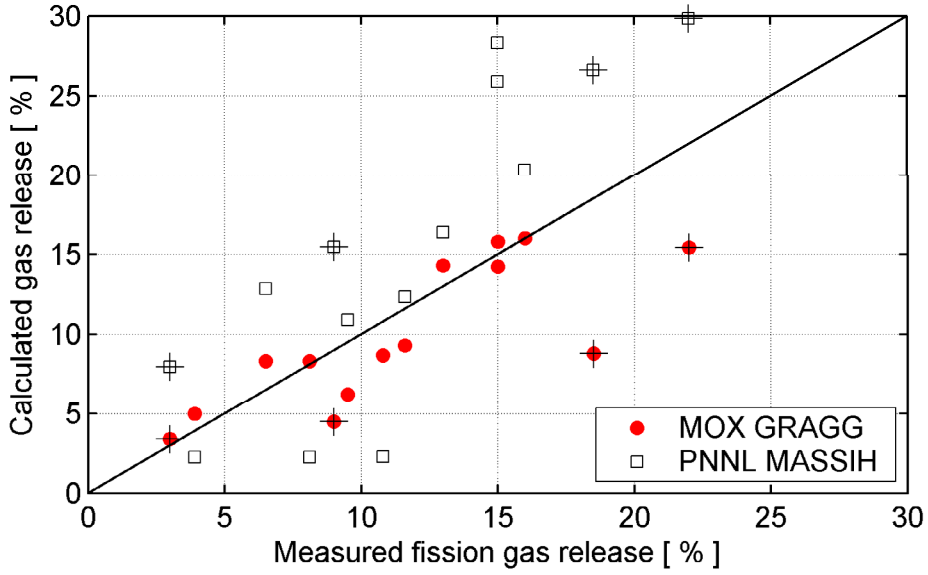

Figure 4.1: Calculated versus measured fission gas release. The figure shows the data presented in table 4.1, excluding the homogeneous material assumption. Data points marked with a cross refer to IFA-629.1 rod 2.

A comparison of measured and calculated fission gas release as a function of burnup is shown for IFA-597 rod 10 in figure 4.2 and for rod 11 in figure 4.3. The plotted results span the entire irradiation life of these rodlets. Calculated results from FRAPCON-3.3 are shown for both the MOX GRAGG and the PNNL MASSIH fission gas release model. The latter model obviously overestimates the gas release early in life for these two rods. However, beyond 15 MWd(kgHM)$^{-1}$, the model captures the trend in data successfully. The results of the MOX GRAGG model follows the measured time history fairly well throughout the entire irradiation history, although the gas release beyond 34 MWd(kgHM)$^{-1}$ is slightly overestimated for rod 11.

Figure 4.4 shows the measured and calculated fission gas release versus time for rod 2 in IFA-629.1. Since the fission gas release during the pre-irradiation in St Laurent B1 was negligible, results are plotted only for the Halden reactor irradiation. Both fission gas release models capture the onset of gas release fairly well, but the released amount of gas is not accurately calculated; the PNNL MASSIH model overestimates the gas release, whereas the opposite is true for the MOX GRAGG model. Moreover, the differences between calculated and measured gas release are much larger for this assessment case than for the IFA-597 rodlets. A comment should also be made on the gas release from 60 up to 150 days: the slow gas release in this period is correctly reproduced with the MOX GRAGG, but not with the PNNL MASSIH model.

Figure 4.5 shows the measured and calculated fission gas release versus time for rod 6 in IFA-629.3. The plot shows the entire Halden reactor irradiation history for the rodlet, even if gas release occurs predominantly during the late, high power, part of the irradiation; see section A.4 in appendix A.

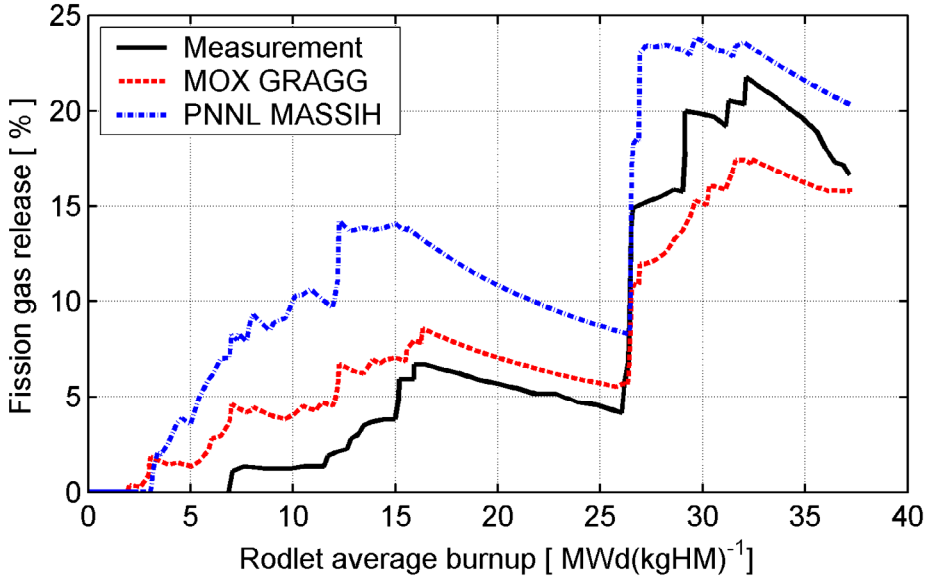

Figure 4.2: Calculated fission gas release fraction versus burnup, in comparison with measurements for IFA-597 rod 10.

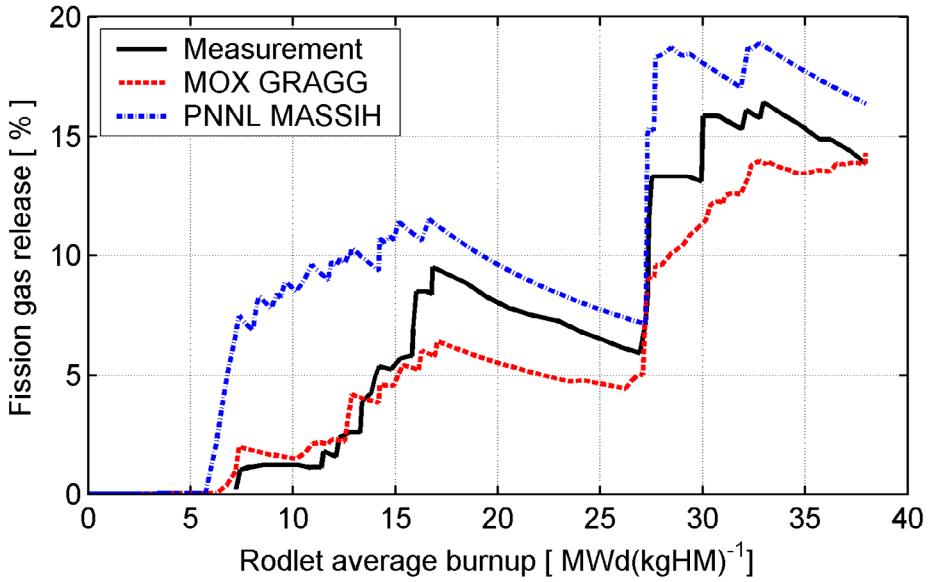

Figure 4.3: Calculated fission gas release fraction versus burnup, in comparison with measurements for IFA-597 rod 11.

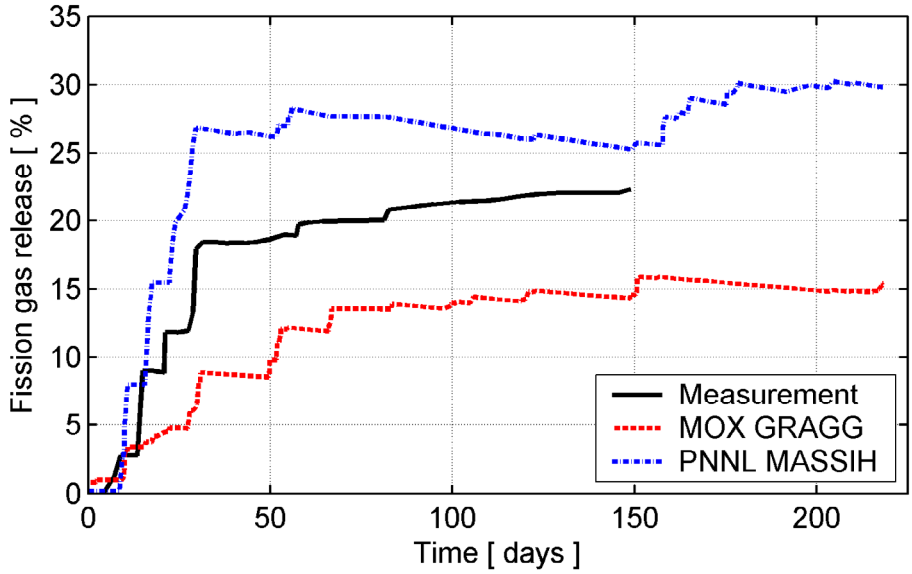

Figure 4.4: Calculated fission gas release fraction versus time, in comparison with measurements for IFA-629.1 rod 2.

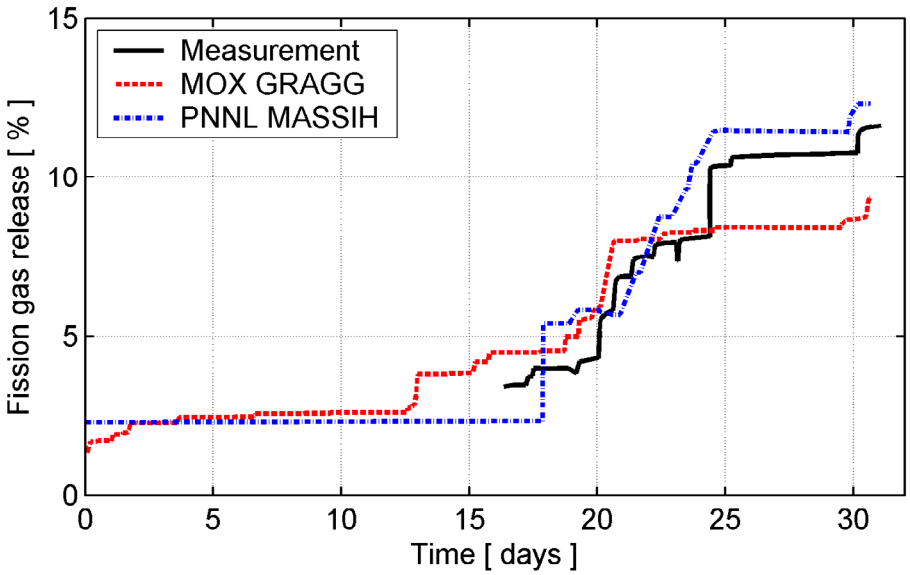

Figure 4.5: Calculated fission gas release fraction versus time, in comparison with measurements for IFA-629.3 rod 6.

4.2 Calculated effect of MOX fuel heterogeneity on FGR

The calculated effect of MOX fuel heterogeneity on fission gas release is illustrated in table 4.1 for the fuel rods included in the assessment database. The rightmost column shows the fission gas release fractions, calculated for a hypothetical material with a homogeneous plutonium distribution. By comparing these results with those of the MOX GRAGG model, in which the heterogeneity effect is considered, we conclude that the effect of heterogeneity is insignificant for the two IFA-597 rodlets and also for the IFA-629.1 rodlet. The reason is that these rodlets are charged with fuel having fairly homogeneous distributions of plutonium, and with respect to fission gas release, the materials are regarded as homogeneous; see eq. (2.6). The strongest effect of heterogeneity is seen for the IFA-629.3 rodlet, the fuel of which is characterized by fairly large plutonium-rich agglomerates and a low average concentration of plutonium; see table A.1 in appendix A.

Figure 4.6 shows the results of a parametric study, in which the MOX GRAGG model has been used to calculate the end-of-life (EOL) fission gas release fraction for three of the Halden test rods, assuming average agglomerate radii from 0 to 60 µm. The measured as-fabricated average agglomerate radii for the MOX fuel in these rods were 7.58 and 8.35 µm, respectively; these values are indicated by the dots in figure 4.6.

As long as the agglomerate radius is below the threshold defined in eq. (2.6), the material is treated as homogeneous by the fission gas release model. As shown in figure 4.6, the threshold is higher for the IFA-597 rodlets than for the IFA-629.3 rod, due to their higher as-fabricated concentration of plutonium.

When the agglomerate radius exceeds the heterogeneity threshold, the calculated end-of-life gas release increases significantly. The calculated end-of-life release fractions for the IFA-597 rods tend asymptotically to 26-27 %, as the agglomerate size increases. For the IFA-629.3 rodlet, the calculated end-of-life gas release reaches a maximum for R_a=20 µm. A possible explanation to this unexpected behaviour is that gas release in the IFA-629.3 high burnup rodlet occurs during an end-of-life power transient, and not during the entire irradiation history, as is the case for the two IFA-597 rods; confer figures 4.2, 4.3 and 4.5. As discussed in section 2.3, the fission rate enhancement factors for plutonium-rich agglomerates and matrix tend to unity at high burnup.

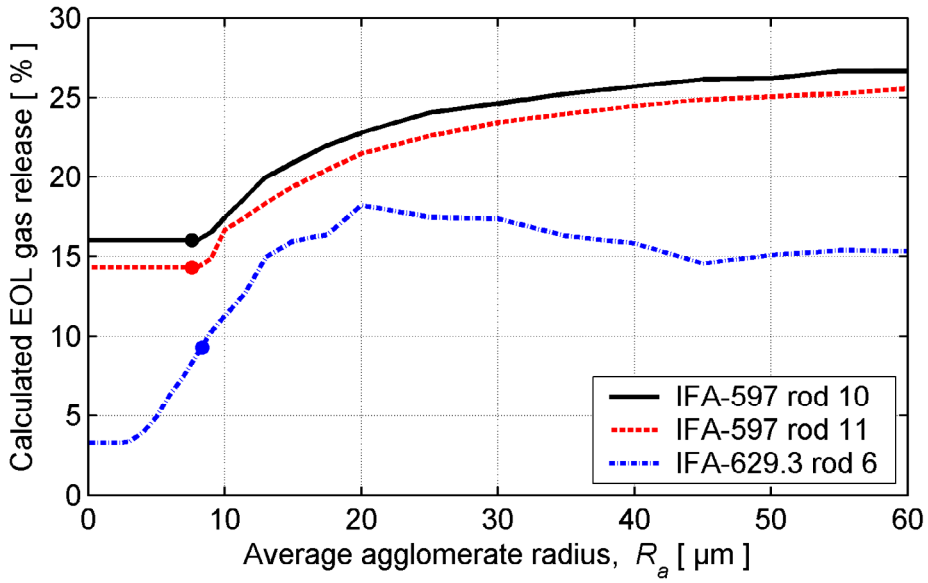

Figure 4.6: Calculated impact of average agglomerate radius on end-of-life fission gas release fraction for three of the Halden test rods. The calculations were done with the FRAPCON-3.3 computer code, using the MOX GRAGG fission gas release model.

4.3 Calculated effect of heterogeneity on fuel densification

Oxide nuclear fuels like UO_2 and MOX undergo densification during the early stages of reactor irradiation. The densification, i.e. the increase in bulk density, is caused by shrinkage and disappearance of fine (<2-3 µm) pores (Small, 1986). These processes can be theoretically modelled by relating pore shrinkage to thermal and fission induced generation of point defects (vacancies and interstitials) and the subsequent migration of these defects to sinks, such as grain boundaries. The reader is referred to the works of Assmann & Stehle (1978), Dollins & Nichols (1978), Lindman (1977) and Hwang et al. (1985) for examples of such theoretical densification models. Models typically used in fuel performance computer codes are, however, much simpler and empirically based. Experience has shown that theoretical densification models are superior to simple correlations only when they can be supplied with detailed material property data as input, and this is generally not the case.

The degree of in-reactor densification varies considerably between fuel materials, depending largely on differences in their as-fabricated grain size and pore size distributions (Freshley et al., 1976). The densification behaviour for a particular material is controlled by temperature and fission rate. One would therefore expect a difference between MOX and UO_2 fuels, because of the local enhancement of temperature and fission rate in the plutonium-rich agglomerates of the MOX material. Recent data on MIMAS AUC MOX fuel suggest that in-reactor densification of this fuel continues over a longer period of time and becomes twice as large as normally seen in UO_2, probably as a result of the heterogeneous distribution of fissile material (Garcia et al., 2000). On the other hand, early experiments (Freshley et al., 1979) show that MOX and UO_2 fuels are comparable with respect to in-reactor densification behaviour.

Here, we will attempt to model the effect of MOX fuel heterogeneity on densification, following the same approach as in the proposed fission gas release model. Hence, the densification of plutonium-rich agglomerates and fuel matrix is treated separately, considering the difference in fission rate and burnup between the two phases. The total densification, $\Delta\rho$, of the material is then calculated by weighting the contribution from each phase with respect to its volume fraction

$$\Delta\rho \quad = \quad v_e \, \Delta\rho_e \quad + \quad (1 - v_e) \, \Delta\rho_m \ . \tag{4.1}$$

Here, $\Delta\rho_e$ and $\Delta\rho_m$ are the changes of density [kgm^{-3}] of equivalent agglomerates and fuel matrix, respectively. They are in our example calculated from the same empirical model, but separate input data are used for the two material components. The applied densification model is the one used for both MOX and UO_2 fuel in FRAPCON-3.3; see appendix B for a full description of this model.

The material in our example is a typical MIMAS AUC MOX fuel, with an isotope composition as defined in table 2.2. As in previous examples, we use w_h=0.06, w_m=0.03 and w_a=0.15 for the plutonia weight fractions; see section 2.1. The agglomerate average radius, R_a, is here assumed to be 8 μm, and λ=2.55 μm. With these data, it follows from eqs. (2.4) and (2.5) that w_e=0.082 and v_e=0.57. Fission rate enhancement factors for the equivalent agglomerates and the fuel matrix are calculated through the procedure described in section 2.2. For the considered fuel material in un-irradiated state, p_e=1.36 and p_m=0.51. Burnup related changes to these values will here be neglected, since we are concerned with early-in-life densification.

The densification of equivalent agglomerates and fuel matrix, calculated through the FRAPCON-3.3 model in appendix B, is plotted with respect to fuel average burnup in figure 4.7. In the calculations, it was assumed that the maximum densification of Pu-rich agglomerates was the same as for the fuel matrix, namely 0.85 %. This value is based on data for MIMAS AUC MOX fuel, presented by Caillot et al. (1997).

The total densification of the heterogeneous MOX material, calculated through eq. (4.1) and the results in figure 4.7, is plotted in figure 4.8. The calculated densification for a homogeneous material is included for comparison. Obviously, there is only a small effect of MOX fuel heterogeneity on the calculated in-reactor densification behaviour.

The difference between the two curves in figure 4.8 is insignificant, in comparison with the large scatter associated with experimental data for in-reactor fuel densification; see e.g. figure B.1 in appendix B. Hence, there is no point in modifying the current FRAPCON-3.3 densification model to include the effect of MOX fuel heterogeneity.

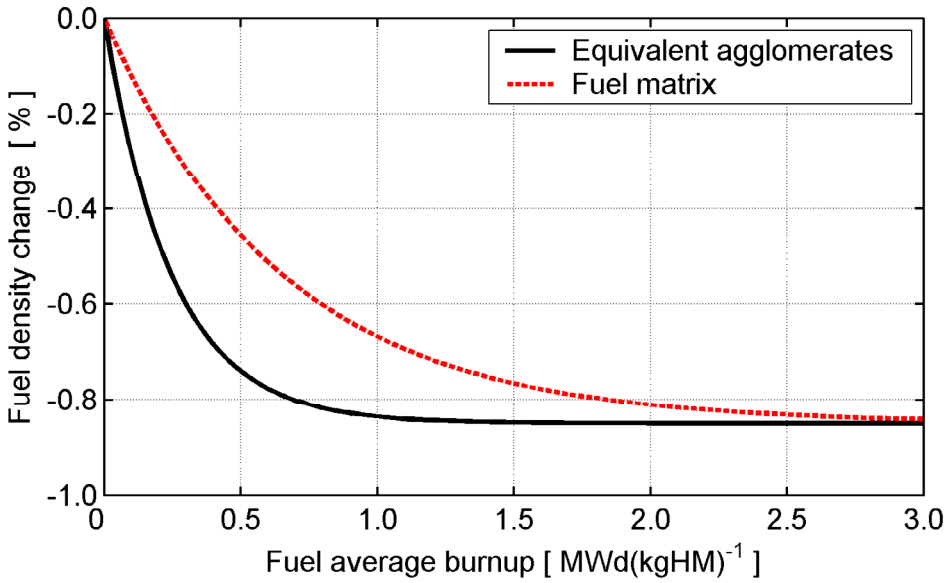

Figure 4.7: Calculated densification of equivalent agglomerates and fuel matrix in typical MIMAS AUC MOX fuel. The calculations were done with the FRAPCON-3.3 densification model, using beginning-of-life values for local fission rate enhancement factors.

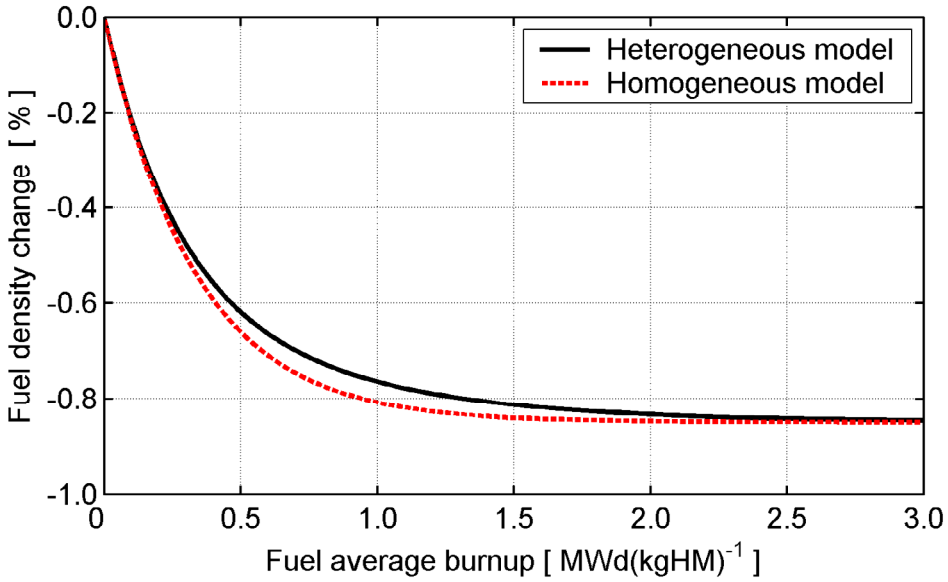

Figure 4.8: Calculated effect of MOX heterogeneity on fuel densification.

4.4 Discussion

Fission gas release from the heterogeneous MOX fuel material is in the proposed model calculated by weighting the contributions from plutonium-rich agglomerates and fuel matrix based on the volume fraction of each phase, as defined by the "rule of mixture" in eq. (2.22). As mentioned already in section 1, this approach is justified only in case i) there is no exchange of fission gas between the phases, ii) the release of gas from phase A is unaffected by the presence of phase B, and vice versa.

The first of these limitations is evaded by introducing equivalent agglomerates in our model, thereby accounting for the migration of fission gas from the agglomerates to the matrix. However, the second limitation remains. Since most of the plutonium-rich agglomerates are embedded in the matrix material and far from a free surface, most of the fission gas generated in the agglomerates must be released *via* the matrix. Hence, the agglomerates are certainly important for the *generation* of fission gas, but the *release* may be controlled by processes taking place predominantly in the matrix. This has been pointed out by several investigators, based on the results of detailed post-irradiation studies of MOX fuel; see e.g. the works of Goll et al. (1993) and Guerin et al. (2000).

The confining role of the fuel matrix provides a possible explanation to why the fission gas diffusivity in MOX fuel has to be reduced relative to UO_2 in our model, as described in section 3.3.2. The reduction is necessary, since we incorrectly assume that the agglomerates, characterized by high fission rate and diffusivity, are equally important to the gas release as the matrix, which has a low fission rate and diffusivity. Hence, it seems that less weight should be given to the agglomerates in calculations of diffusion-controlled gas release.

Another issue concerns the geometrical modelling of agglomerates in the mixed oxide fuel material. The plutonium-rich agglomerates are in the proposed model represented by a population of spherical particles of equal size. This particle size is in our calculations set equal to the average agglomerate size, which is usually measured in image analysis by the mean linear intercept method. Using the average size may not be the best option, considering the complex relation between agglomerate size and calculated fission gas release shown in figure 4.6. A more rigorous approach would be to consider the agglomerate size distribution, instead of using a single particle size in the model. This can be done fairly simply by multiply calling the proposed model within a loop over a number of particle sizes. The fission gas release is then calculated by weighting the results for each particle size based on the measured agglomerate size distribution of the material. The approach, which has been used by Koo et al (2002), comes at the expense of increased computational cost and processing time.

5 Conclusions

A computational model for fission gas release from heterogeneous MOX fuel has been developed, implemented in the FRAPCON-3.3 fuel performance program, and validated against experimental data. The model is similar to the one proposed by Koo et al. (2000), in so far that it uses the concept of equivalent plutonium-rich agglomerates, embedded in a plutonium-lean matrix, to represent the heterogeneous MOX material. However, the fission gas release from the two phases of the material is treated with the GRAGG model by Forsberg & Massih (2001,2007), and in contrast to Koo and co-workers, we consider burnup related changes to the isotope composition of both agglomerates and matrix.

The model has been verified and calibrated against fission gas release data for six PWR fuel rods, all of which were charged with MIMAS type mixed oxide fuel. The rods were tested in the Halden reactor, and instrumented with pressure transducers for on-line measurements of fuel fission gas release with respect to time under irradiation. The end-of life rod average burnup and fission gas release range from 37 to 60 $MWd(kgHM)^{-1}$ and 12 to 22 %, respectively.

Fission gas release fractions calculated with the proposed model agree closely with measurements for five of the six fuel rods. The exception is rod 2 of IFA-629.1, for which the fission gas release is significantly underestimated. Yet, the overall impression is that the proposed model reproduces the measured data from the experiments more accurately than the standard gas release model for MOX fuel in FRAPCON-3.3.

Parametric studies with the proposed model show that MOX fuel fission gas release increases with increasing size of the plutonium-rich agglomerates. This result is also supported by experimental data (Billaux & van Vliet, 1986). However, the trend between agglomerate size and gas release is not seen for small agglomerates, and according to our model, the MOX fuel material can be viewed as homogeneous with regard to fission gas release when the agglomerate size is below a certain threshold. The calculated threshold size depends on fuel plutonium content and the distribution of plutonium between agglomerates and fuel matrix. For typical MIMAS AUC MOX fuel, the calculated agglomerate threshold size is about 15 μm.

The heterogeneous plutonium distribution in MOX fuel may affect not only fuel fission gas release, but also the in-reactor deformation behaviour. Densification of MOX fuel was therefore studied with a composite material approach, similar to the one used in our fission gas release model. The calculated impact of MOX fuel heterogeneity on in-reactor densification was found to be small, but it should be remarked that this conclusion is based on rough calculations with the empirical densification model in FRAPCON-3.3, and a more rigorous analysis is warranted. However, such an analysis is difficult to perform, since open literature data on in-reactor densification of modern MOX fuel materials are scarce.

Although the proposed fission gas release model successfully reproduces most of the experiments in the considered database, there are some extensions and improvements to suggest for the future:

- Firstly, a more consistent modelling of fuel re-structuring at high burnup and its effect on fission gas release is desirable. The current re-structuring model treats the fuel material as homogeneous (Jernkvist & Massih, 2005). For MOX fuel, the model should be changed to consider plutonium-rich agglomerates and matrix apart, since re-structuring occurs first and foremost in the agglomerates.
- Secondly, it would be interesting to extend the gas release model to account for the agglomerate size distribution, instead of using just a single (average) agglomerate size in the calculations. This extension can be fairly easily done, but it should be remarked that verification and calibration of such a model would require in-reactor fission gas release experiments performed on MOX fuel materials with well-characterized microstructures. It is unclear whether such data are available in literature.

6 References

Assmann, H. and Stehle, H., 1978.
Thermal and in-reactor densification of UO_2: mechanisms and experimental results,
Nuclear Engineering and Design, 48, pp 49-67.

Billaux, M. and van Vliet, J., 1986.
Impact of fuel heterogeneities on fission gas release for LWR U-Pu mixed oxide fuels,
Res Mechanica, 17, pp 41-57.

Boulanger, D., Lippens, M., Mertens, L., Basselier, J. and Lance, B., 2004.
High burnup PWR and BWR MOX fuel performance: A review of BELGONUCLEAIRE recent experimental programs, Proc. 2004 International Meeting on Light Water Reactor Fuel Performance, Orlando, Florida, USA, September 19-22, 2004, pp 273-283.

Caillot, L., Chotard, A. and Berton, J.P., 1997.
Analytical studies of the behaviour of MOX fuel,
Proc. 1997 International Topical Meeting on LWR Fuel Performance, Portland, Oregon, USA, March 2-6, 1997, pp 62-69.

Claudel, J. and Huet, F., 2001.
Results from the burnup accumulation test with high exposure (63 MWd/kgHM) MOX fuel (IFA-648), OECD Halden Reactor Project Report HWR-651, Halden, Norway.

Dollins, C.C. and Nichols, F.A., 1978.
In-pile intragranular densification of oxide fuels,
Journal of Nuclear Materials, 78, pp. 326-335.

Fisher, S.B., White, R.J., Cook, P.M.A., Bremier, S., Corcoran, R.C., Stratton, R., Walker, C.T., Ivison, P.K. and Palmer, I.D., 2002.
Microstructure of irradiated SBR MOX fuel and its relationship to fission gas release,
Journal of Nuclear Materials, 306, pp. 153-172.

Forsberg, K. and Massih, A.R., 2001.
Theory of fission gas release during grain growth,
Transactions of the 16th International Conference on Structural Mechanics in Reactor Technology (SMiRT 16), Washington D.C., USA, August 12-17, 2001.

Forsberg, K. and Massih, A.R., 2007.
Kinetics of fission product gas release during grain growth,
Modelling and Simulation in Materials Science and Engineering, 15(3), pp 335-353.

Freshley, M.D., Brite, D.W., Daniel, J.L. and Hart, P.E., 1976.
Irradiation-induced densification of UO_2 pellet fuel,
Journal of Nuclear Materials, 62, pp. 138-166.

Freshley, M.D., Brite, D.W., Daniel, J.L. and Hart, P.E., 1979.
Irradiation-induced densification and PuO_2 particle behavior in mixed oxide pellet fuel,
Journal of Nuclear Materials, 81, pp. 63-92.

Garcia, P., Boulore, A., Guerin, Y., Trotabas, M. and Goeuriot, P., 2000.
In-pile densification of MOX fuels in relation to their initial microstructure,
Proc. ANS Topical Meeting on Light Water Reactor Fuel Performance, Park City, Utah, USA, April 10-13, 2000.

Goll, W., Fuchs, H.P., Manzel, R. and Schlemmer, F.U., 1993.
Irradiation behavior of UO_2/PuO_2 fuel in light water reactors,
Nuclear Technology 102, pp 29-46.

Guerin, Y., Noirot, J., Lespiaux, D., Struzik, C., Garcia, P., Blanpain, P. and Chaigne, G., 2000. *Microstructure evolution and in-reactor behaviour of MOX fuel*,
Proc. ANS Topical Meeting on Light Water Reactor Fuel Performance, Park City, Utah, USA, April 10-13, 2000.

Hagrman, D. L., Reymann, G.A. and Mason, G.E., 1981.
A handbook of materials properties for use in the analysis of light water reactor fuel rod behavior, MATPRO Version 11 (Revision 2), NUREG/CR-0479 (TREE-1280), prepared by EG&G Idaho, Inc., Idaho Falls, Idaho for the U.S. Nuclear Regulatory Commission, Washington, D.C., USA, 1981.

Hwang, W., Seo, K.S. and Suk, H.C., 1985.
A mechanistic model for in-reactor densification of UO_2,
Journal of the Korean Nuclear Society, 17(2), pp 116-128.

IAEA, 2003.
Status and advances in MOX fuel technology,
International Atomic Energy Agency, Technical report series 415, Vienna, Austria.

Ishida, M. and Korei, Y., 1994.
Modeling and parametric studies of the effect of Pu-mixing heterogeneity on fission gas release from mixed oxide fuels of LWRs and FBRs,
Journal of Nuclear Materials, 210, pp 203-215.

Jernkvist, L.O., 2005.
The FRAPCON-3.3 computer code – SKI version,
Quantum Technologies technical report TR05-008, December 2005.

Jernkvist, L.O., 2008.
The SKI version of the FRAPCON-3.3 computer code: FRAPCON-3.3.1-SKI,
Quantum Technologies technical report TR08-001, January 2008.

Jernkvist, L.O. and Massih, A.R., 2002.
Analysis of the effect of UO_2 high burnup microstructure on fission gas release,
Swedish Nuclear Power Inspectorate (SKI) research report 02:56, October 2002.

Jernkvist, L.O. and Massih, A.R., 2005.
Models for fuel rod behaviour at high burnup,
Swedish Nuclear Power Inspectorate (SKI) research report 2005:41, December 2004.

Koike, H., 2004.
The MOX fuel behaviour test IFA-597.4/.5/.6/.7: Summary of in-pile fuel temperature and gas release data,
OECD Halden Reactor Project Report HWR-729, Halden, Norway.

Koo, Y.H., Sohn, D.S. and Strijov, P., 2000.
A fission gas release model for MOX fuel and its verification,
Proc. International Symposium on MOX Fuel Cycle Technologies for Medium and Long-Term Deployment, Vienna, Austria, May 17-21, 1999, International Atomic Energy Agency, Report IAEA-CSP-3/P, June 2000, pp 500-507.

Koo, Y.H., Lee, B.H., Cheon, J.S., and Sohn, D.S, 2002.
Modeling and parametric studies of the effect of inhomogeneity on fission gas release in LWR MOX fuel, Annals of Nuclear Energy, 29, pp 271-286.

Lanning, D. D., Beyer, C. E. and Painter, C. L., 1997a.
FRAPCON-3: Modifications to fuel rod material properties and performance models for high-burnup application,
NUREG/CR-6534, PNNL-11513, Vol. 1, prepared for the U.S. Nuclear Regulatory Commission by Pacific Northwest National Laboratory, Richland, Washington, USA.

Lanning, D. D., Beyer, C. E. and Berna, G. A., 1997b.
FRAPCON-3: Integral assessment,
NUREG/CR-6534, PNNL-11513, Vol. 3, prepared for the U.S. Nuclear Regulatory Commission by Pacific Northwest National Laboratory, Richland, Washington, USA.

Lanning, D. D., Beyer, C. E. and Geelhood, K. J., 2005.
FRAPCON-3 updates, including mixed-oxide fuel properties,
NUREG/CR-6534, PNNL-11513, Vol. 4, prepared for the U.S. Nuclear Regulatory Commission by Pacific Northwest National Laboratory, Richland, Washington, 2005.

Lassmann, K., O'Carroll, C., van de Laar, J. and Walker, C.T., 1994.
The radial distribution of plutonium in high burnup UO_2 fuels,
Journal of Nuclear Materials, 208, pp 223-231.

Lassmann, K., Walker, C.T. and van de Laar, J., 1998.
Extension of the TRANSURANUS burnup model to heavy water reactor conditions,
Journal of Nuclear Materials, 255, pp 222-233.

Lindman, N., 1977.
On the rate of in-reactor UO_2 densification,
Journal of Nuclear Materials, 71, pp 73-77.

Massih, A.R., 2006.
Models for MOX fuel behaviour: A selective review,
Swedish Nuclear Power Inspectorate (SKI) research report 2006:10, January 2006.

Matzke, Hj., 1982.
Radiation damage in crystalline insulators, oxides and ceramic nuclear fuels,
Radiation Effects, 64, pp 3-33.

Matzke, Hj., 1995.
The rim-effect in high burnup UO_2 nuclear fuel,
In P. Vincenzini (ed), Ceramics: Charting the Future, Proc. World Ceramics Congress, Florence, Italy, June 28 - July 4, 1995, pp 2913-2920.

Mertens, L. and Lippens, M., 2001.
Study of fission gas release on high burnup MOX fuel,
Proc.of the ENS TopFuel 2001 conference, May 27-30, 2001, Stockholm, Sweden.

Nishi, M. and Lee, B.H., 2001.
Summary of pre-irradiation data on fuel segments supplied by EdF/Framatome and tested in IFA-610, 629 and 648,
OECD Halden Reactor Project Report HWR-664, Halden, Norway.

Olander, D.R., 1976.
Fundamental aspects of nuclear reactor fuel elements,
TID-26711-P1, National Technical Service, U. S. Department of Commerce, Springfield, Virginia, USA, 1976.

Petitprez, B., 2002.
Ramp tests with two high burnup MOX fuel rods in IFA-629.3,
OECD Halden Reactor Project Report HWR-714, Halden, Norway.

Rolstad, E., Hanevik, A. and Knudsen, K.D., 1974.
Measurements of the length changes of UO_2 fuel pellets during irradiation,
Proc. of the Enlarged Halden Programme Group Meeting on Computer Control and Fuel Research, Sandefjord, Norway, June 4-7, 1974. Halden project report HPR-188.

Sauer, G. and Besenböck, W., 2007.
Estimation of the influence of plutonium agglomerates in MOX fuel on the pellet temperature, Proc. 2007 International Light Water Reactor Fuel Performance Meeting, San Fancisco, California, USA, September 30 – October 3, 2007.

Small, G.J., 1986.
Densification of uranium dioxide during thermal reactor irradiation,
Res Mechanica, 18, pp 51-93.

Spino, J., Vennix, K. and Coquerelle, M., 1996.
Detailed characterization of the rim microstructure in PWR fuels in the burn-up range 40-67 GWd/tM, Journal of Nuclear Materials, 231, pp 179-190.

Stacey, W.M., 2001.
Nuclear reactor physics,
John Wiley & Sons, Inc., New York, USA.

Takahashi, K., Kamimura, K., Yamaguchi, T. and Masuda, S., 1988.
Development of quality control data base "DANTE" and relational analysis between fission gas release behavior and plutonium homogeneity in mixed oxide fuel by DANTE,
Journal of Nuclear Materials, 153, pp 232-238.

Turnbull, J.A., Friskney, C.A., Findlay, J.R., Johnson, F.A. and Walter, A.J., 1982.
The diffusion coefficient of gaseous and volatile species during the irradiation of uranium dioxide, Journal of Nuclear Materials, 107, pp 168-184.

Walker, C.T., Coquerelle, M., Goll, W. and Manzell, R., 1991.
Irradiation behaviour of MOX fuel: Results of an EPMA investigation,
Nuclear Engineering and Design, 131, pp 1-16.

Walker, C.T., Goll, W. and Matsumura, T., 1996.
Effect of inhomogeneity on the level of fission gas and caesium release from OCOM MOX fuel during irradiation, Journal of Nuclear Materials, 228, pp 8-17.

Walker, C.T., Goll, W. and Matsumura, T., 1997.
Further observations on OCOM MOX fuel: microstructure in the vicinity of the pellet rim and fuel-cladding interaction, Journal of Nuclear Materials, 245, pp 169-178.

White, R.J., 1999.
The re-irradiation of MIMAS-MOX fuel in IFA-629.1,
OECD Halden reactor project report HWR-586, Halden, Norway.

White, R.J., 2000.
Fission gas release,
OECD Halden reactor project report HWR-632, Halden, Norway.

White, R. J., Fischer, S.B., Cook, P.M.A., Stratton, R., Walker, C.T. and Palmer, I.D., 2001. *Measurement and analysis of fission gas release from BNFL's SBR MOX fuel*,
Journal of Nuclear Materials, 288, pp 43-56.

Appendix A: Assessment cases for MOX fuel fission gas release

The database used for assessment and calibration of the proposed MOX fuel fission gas release model comprise data from six instrumented MOX fuel rodlets, tested in the Halden heavy water reactor, Norway. The rodlets were irradiated in four different instrumented fuel assemblies (IFAs) in the Halden reactor. Four of the rodlets were re-fabricated from full-length PWR fuel rods, which had been irradiated to high burnup in power generating reactors.

All the considered test rods were of PWR design, with Zircaloy-4 cladding and charged with MOX fuel fabricated through the micronized master blend (MIMAS) process. Many details on the microstructure and plutonium distribution of the considered fuel materials were unfortunately unavailable. For all fuel rods, it has therefore been assumed that the weight fraction of plutonia was 0.15 and 0.03 in the plutonium-rich agglomerates and the fuel matrix, respectively. These values are based on literature data reported for MIMAS AUC fuel (Garcia, et al., 2000) and (Fisher et al., 2002).

The design of each test rod is detailed in table A.1. The pre-irradiation and test conditions are summarized in the following subsections.

A.1 IFA-597.4/5/6/7

Two rodlets charged with MIMAS MOX fuel, fabricated by Nuclear Fuel Industries (NFI) in Japan, were irradiated in the Halden test reactor to a burnup of 37-38 MWd(kgHM)$^{-1}$. The rodlets were operated at Halden reactor coolant conditions, i.e. at a pressure of 3.4 MPa and a temperature of 500-510 K. The irradiation took place from 1997 to 2002 in four different instrumented fuel assemblies, denoted IFA-597.4/5/6/7. While IFA-597.4 and IFA-597.6 contained only the two MOX rodlets, the other two IFAs comprised also some UO_2 rodlets (Koike, 2004).

Each of the MOX fuel rodlets was instrumented with a fuel centre thermocouple and an internal pressure transducer. The rodlets, denoted rod 10 and rod 11, were of almost identical design, typical for fuel rods in 17×17 PWR fuel assemblies. The only difference between the rodlets was the fuel pellet design; rod 10 was charged with 10.7 mm long solid pellets, whereas rod 11 contained 10.5 mm long annular pellets. The central hole of the annular pellets was 1.8 mm in diameter (Koike, 2004).

The irradiation of IFA-597.4/5/6/7 was aimed to investigate the thermal behaviour and fission gas release of MOX fuel and to explore potential differences between solid and annular MOX fuel pellets. Power upratings, each followed by a period with relatively high power, were performed at burnup intervals of about 10 MWd(kgHM)$^{-1}$ to study fission gas release: the gas release was monitored on-line through the pressure transducers in the rodlets.

Rodlet design		**IFA-597 Rod 10**	**IFA-597 Rod 11**	**IFA-606 Rod sg**	**IFA-606 Rod lg**	**IFA-629.1 Rod 1**	**IFA-629.1 Rod 2**	**IFA-629.3 Rod 5**	**IFA-629.3 Rod 6**
Type of mother rod		PWR 17x17	PWR 17x17	PWR 14x14	PWR 14x14	PWR 17x17	PWR 17x17	PWR 17x17	PWR 17x17
Active length	[mm]	224	220	398	398	381	451	454	451
Free volume, cold	[cm^3]	3.00	3.30	3.91	3.91	2.81	3.31	2.81	2.74
Gas fill pressure	[MPa]	0.50	0.50	0.51	0.51	2.60	2.60	2.60	2.60
Cladding design									
Outer diameter	[mm]	9.50	9.50	10.72	10.72	9.50	9.50	9.50	9.50
Thickness	[mm]	0.64	0.64	0.62	0.62	0.57	0.57	0.57	0.57
Fuel pellet design									
Diameter	[mm]	8.04	8.04	9.29	9.29	8.19	8.19	8.19	8.19
Inner diameter	[mm]	0	1.80	0	0	0	0	0	0
Height	[mm]	10.70	10.50	12.56	12.56	11.86	11.86	11.93	11.90
Density, in % of theoretical	[%]	95.86	95.86	95.59	95.59	95.34	95.34	94.72	94.62
Grain size	[µm]	5.45	5.45	8.00	11.00	11.70	11.70	8.50	6.75
Pu agglomerate radius	[µm]	7.58	7.58	(8.0)	(8.0)	3.48	3.48	7.80	8.35
Oxygen-to-metal ratio	[-]	1.999	1.999	(1.999)	(1.999)	1.998	1.998	1.996	2.000
Plutonia content	[wt%]	8.49	8.49	6.01	6.01	5.98	5.98	5.98	4.72
Enrichment (U235/TotalU)	[%]	0.252	0.252	0.278	0.278	0.253	0.253	0.231	0.225

Table A.1: Design of test rods in the Halden reactor IFA-597, IFA-606, IFA-629.1 and IFA-629.3 experiments.
The data are compiled from Halden reactor project reports and other literature sources, as defined in the description of each experiment.
Numbers given within brackets are estimated values, which have been used in our calculations.

The on-line measurements of gas release were confirmed by post-irradiation gas analysis. The end-of-life gas release, determined from mass spectrometry analysis, was 16 and 13 % in rod 10 and 11, respectively (Koike, 2004).

The power histories applied in our simulation of IFA-597.4/5/6/7 with FRAPCON-3.3 are shown in figure A.1. These power histories were generated from plots given in the report by Koike (2004), which, unfortunately, seem to be inconsistent.[4] Hence, the applied power histories are tentative, and should be checked as more reliable data become available from the Halden reactor project.

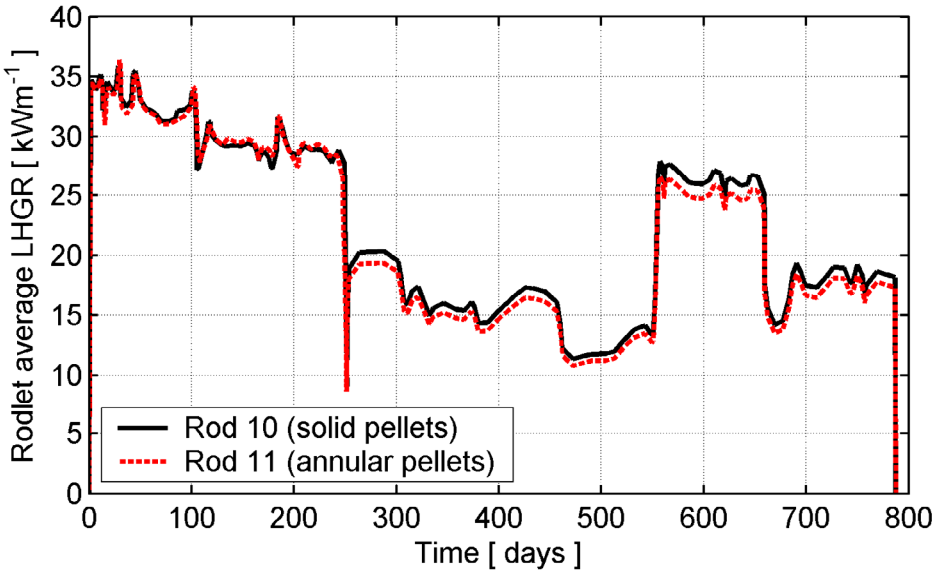

Figure A.1: Power histories for rodlets 10 and 11 in the IFA-597 experiment.

A.2 IFA-606

IFA-606 comprised four short-length test rodlets with MOX fuel, fabricated by Belgonucleaire through the MIMAS AUC process (Mertens & Lippens, 2001). The rodlets were sampled from two full-length mother rods, which had been irradiated at fairly low power to a peak pellet burnup of about 50 MWd(kgHM)$^{-1}$ in the Beznau-1 PWR, Switzerland. The rod average linear heat generation rate (LHGR) was below 23 kWm^{-1}, which resulted in a fission gas release of merely 2 % at end of irradiation in Beznau-1 (Boulanger et al., 2004). Figure A.2 shows the irradiation power histories for the considered segments of the mother rods.

The mother rods were of almost identical design, typical for fuel rods in 14×14 PWR fuel assemblies. The major difference between the mother rods was in the fuel pellet grain size, which was 8 and 11 µm, respectively. An important objective of the Halden IFA-606 experiment was to investigate the influence of MOX fuel as-fabricated grain size on the fission gas release. Two rodlets were sampled from each mother rod.

[4] According to figure 5 in the report by Koike (2004), rod 10 and 11 reach the same end-of-life burnup, although the linear heat generation rate differs significantly between the rods in IFA-597.4.

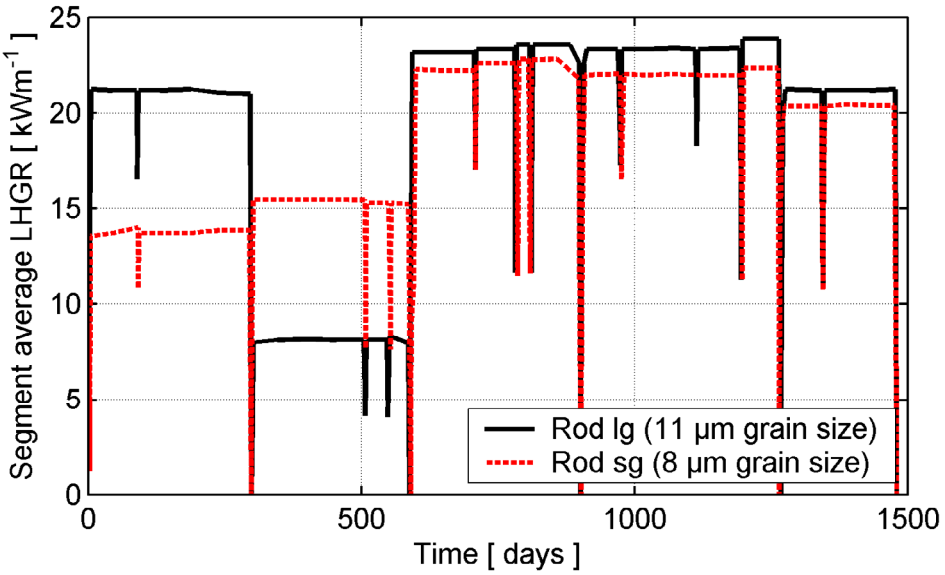

Figure A.2: Power histories for fuel rod segments sampled for the IFA-606 rodlets during base irradiation in the Beznau-1 PWR.

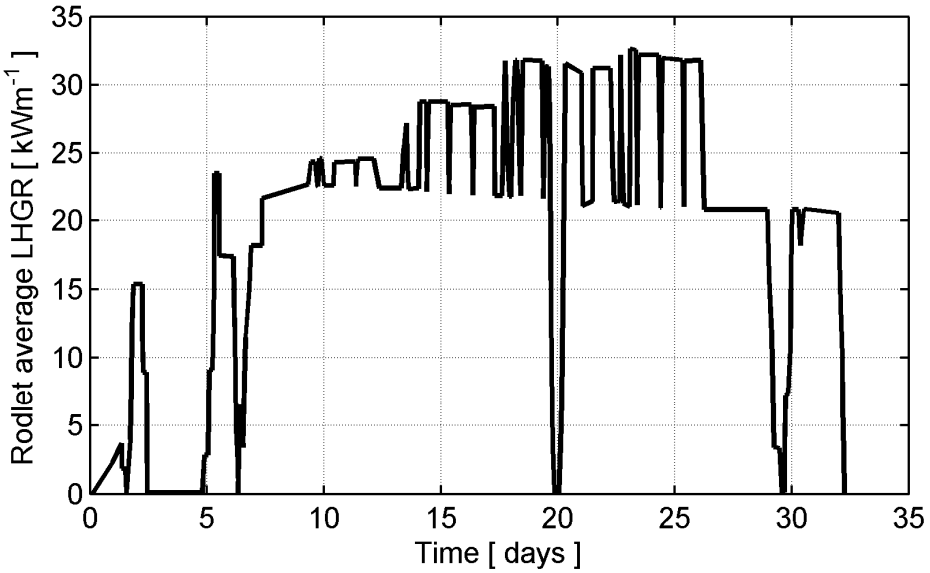

Figure A.3: Power history for the IFA-606 phase 2 experiment in the Halden reactor. The large grain (lg) and small grain (sg) rodlets experienced the same power history.

Each of the re-fabricated rodlets was equipped with a fuel centre thermocouple and a pressure transducer, which made it possible to monitor fission gas release on-line during the Halden reactor irradiation. The correctness of the on-line fission gas release measurements was confirmed by rod puncturing and gas analysis after completed irradiation.

Two different experiments on fuel fission gas release were carried out on IFA-606 in the Halden reactor. In the first experiment, named "phase 1", two of the rodlets were subjected to a short (≈1 day) power history with nine power cycles of increasing amplitude (Mertens & Lippens, 2001). The intention was to study burst release of fission gas, and the possible influence of fuel grain size on this release mechanism. This experiment will not be considered here.

The second experiment, "phase 2", aimed to study diffusion controlled gas release under steady-state conditions. In this experiment, two rodlets with different fuel grain size were irradiated in parallel at high power for about thirty days. The power history included regular returns to short periods of low power, in order to allow pellet-clad gap opening, axial gas pressure equilibration and detection of fission gas release. The power history applied in simulation of the IFA-606 phase 2 experiment is shown in figure A.3. The irradiation took place under Halden reactor cooling conditions i.e. at a pressure of 3.4 MPa and an inlet coolant temperature of 493 K.

The fission gas release during the phase 2 experiment was 13 %, as determined by rod puncturing during post-irradiation examinations (Mertens & Lippens, 2001). The fission gas release was also measured as a function of time during the experiment, but these data are unfortunately unavailable in open literature.

A.3 IFA-629.1

IFA-629.1 comprised two rodlets with MIMAS MOX fuel, fabricated by Belgo-nucleaire. It should be remarked that the fuel pellets of these rodlets were reported to have unusually small plutonium-rich agglomerates: the average size was merely 6.95 μm (Nishi & Lee, 2001).

The rodlets were re-fabricated from the same mother rod, a PWR fuel rod that had been irradiated for two reactor cycles in the St Laurent B1 PWR in France. Figure A.4 shows the St Laurent B1 power histories for the considered fuel rod segments. The average burnups of the sampled segments were 26.8 and 29.3 $MWd(kgHM)^{-1}$, respectively (White, 1999). Both rods were instrumented with fuel centre thermocouples. Rod 1 was also fitted with a rod elongation sensor, whereas rod 2 was equipped with an internal pressure transducer.

After re-fabrication and instrumentation, the rodlets were loaded into the Halden reactor and operated at a coolant pressure of 3.4 MPa and a coolant temperature between 500 and 510 K. The first part of the irradiation was dedicated to on-line measurement of fission gas release as the fuel temperature was increased step-wise through the known threshold for thermal fission gas release of standard UO_2 fuel (White, 1999).

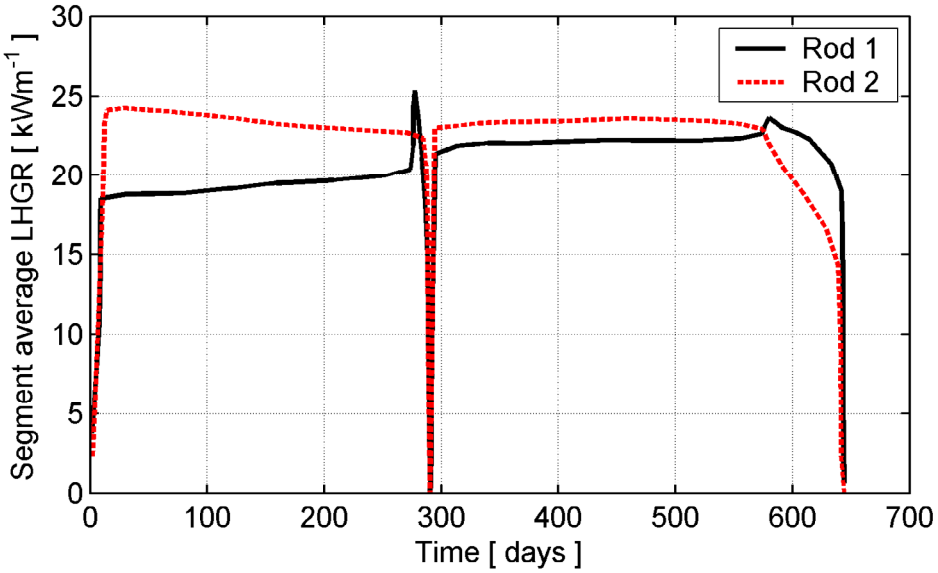

Figure A.4: Power histories for fuel rod segments sampled for the IFA-629.1 rodlets during base irradiation in the St Laurent B1 PWR.

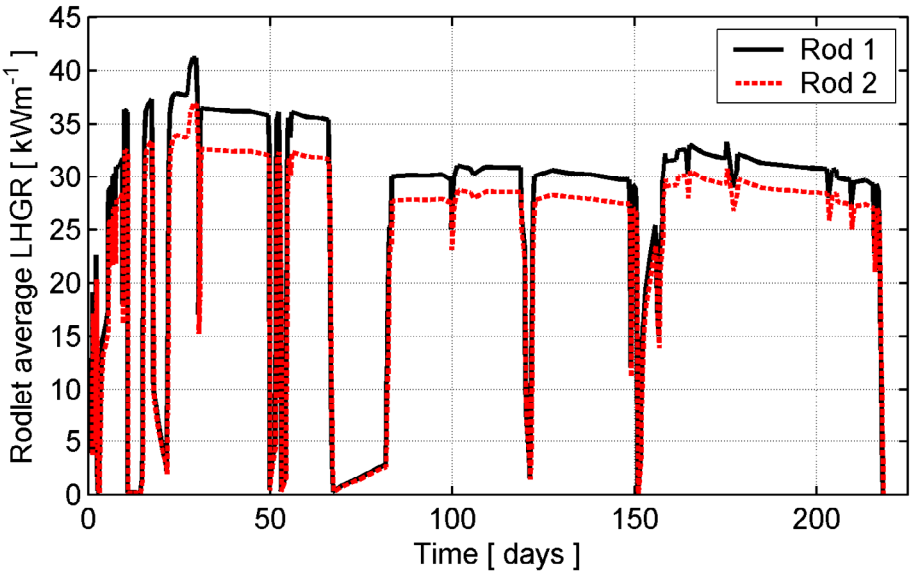

Figure A.5: Rodlet power histories for the IFA-629.1 experiment in the Halden reactor. The rodlets gained 11-12 MWd(kgHM)$^{-1}$ in fuel burnup during this irradiation.

The irradiation was then continued at nearly constant power and temperature, to study fission gas release and thermo-mechanical fuel performance at high power; more precisely, at linear heat generation rates of 30-40 kWm^{-1}. The irradiation in the Halden reactor lasted for about 180 full power days, under which the rodlets gained 11-12 $MWd(kgHM)^{-1}$ in fuel burnup[5]. The test rod power histories for the Halden reactor irradiation are shown in figure A.5.

The internal gas pressure of rod 2 was measured on-line throughout the irradiation in Halden, which made it possible to estimate the fuel fission gas release as a function of time (White, 1999). Moreover, rod 2 was punctured after irradiation, and the end-of-life fission gas release fraction was determined to be 21.7 % (Lanning et al., 2005).

A.4 IFA-648.1/629.3

Two high-burnup rodlets with Begonucleaire MIMAS MOX fuel have been extensively tested in the Halden reactor with respect to thermal performance, deformations and fuel fission gas release under both steady-state reactor operation and transient conditions. The rodlets were sampled from two full-length fuel rods in a 17×17 fuel assembly, which had been irradiated for four reactor cycles in the French Graveline 4 PWR. The final average burnups of the sampled segments were 56.9 and 52.5 $MWd(kgHM)^{-1}$, respectively (Nishi & Lee, 2001) and (Claudel & Huet, 2001). Fuel fission gas release in the two full-length mother rods was 4.86 and 2.58 % (Nishi & Lee, 2001).

The sampled segments were re-fabricated into rodlets with a fuelled length of about 450 mm. Both rodlets were instrumented with fuel centre thermocouples. One of the rodlets was additionally equipped with a rod elongation sensor, whereas the other carried an internal pressure transducer (Claudel & Huet, 2001).

After re-fabrication, the rodlets were irradiated under simulated PWR conditions in a pressurized water loop within the Halden reactor core. This irradiation, performed within IFA-648.1, was aimed to extend the fuel burnup while avoiding significant fission gas release. Hence, the irradiation took place at low power (≈11 kWm^{-1}), and increased the fuel burnup by about 7 $MWd(kgHM)^{-1}$ (Claudel & Huet, 2001). The pre-irradiation histories for the rod segments, including the Graveline 4 operation and the burnup accumulation in Halden IFA-648.1, are shown in figure A.6.

After burnup accumulation in IFA-648.1, the two rodlets were moved to IFA-629.3 for transient testing. The rod designations changed: rod 1 in IFA-648.1 is called rod 5 in IFA-629.3, and rod 2 is called rod 6. It should be remarked that the fuel centre thermocouple and the internal pressure transducer in IFA-648.1 rod 2 were replaced before loading it as rod 6 in IFA-629.3 (Petitprez, 2002).

In contrast to IFA-648.1, IFA-629.3 was irradiated under nominal Halden reactor conditions, i.e. it was placed directly in the heavy water coolant, which had a pressure of 3.4 MPa and a temperature between 500 and 510 K. The irradiation took place in two phases. The instrumented fuel assembly was moved within the core between the phases,

[5] Only part of the irradiation history (120 days) is presented in (White, 1999). The remaining part is given in (Lanning et al., 2005).

resulting in a slight change of cooling conditions and axial power distribution. The irradiation life of the test rodlets is thus fairly complex, since it involves operation under PWR, simulated PWR and Halden reactor conditions. In addition, the rodlet equipped with a pressure transducer (rod 2/6) was re-fabricated twice during its lifetime.

The test performed with IFA-629.3 aimed at establishing the temperature threshold for thermal fission gas release in high-burnup MOX fuel, but it also provided data on thermal performance and pellet-clad mechanical interaction behaviour for such fuel (Petitprez, 2002). The test rod power histories for the Halden reactor irradiation in IFA-629.3 are shown in figure A.7.

The fractional fission gas release in rod 6 during the IFA-629.3 irradiation was 8.6 % (Petitprez, 2002). Based on the measured fission gas release in the full-length mother rod from which this rodlet was sampled (2.58 %), the total fission gas release of rod 6 is estimated to 11.6 %.

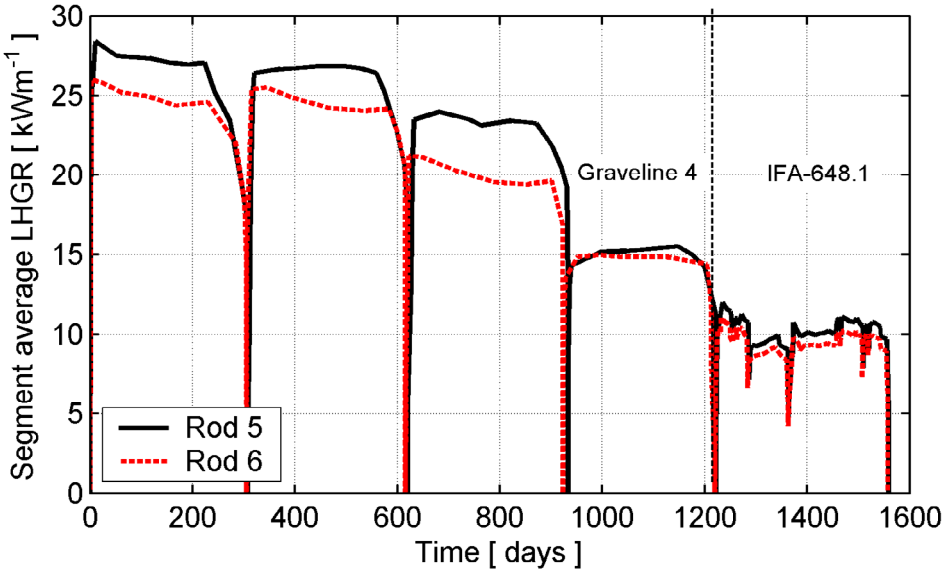

Figure A.6: Power histories for fuel rod segments sampled for the IFA-629.3 rodlets during base irradiation in the Graveline 4 PWR, and the subsequent burnup accumulation irradiation at low power in Halden IFA-648.1.

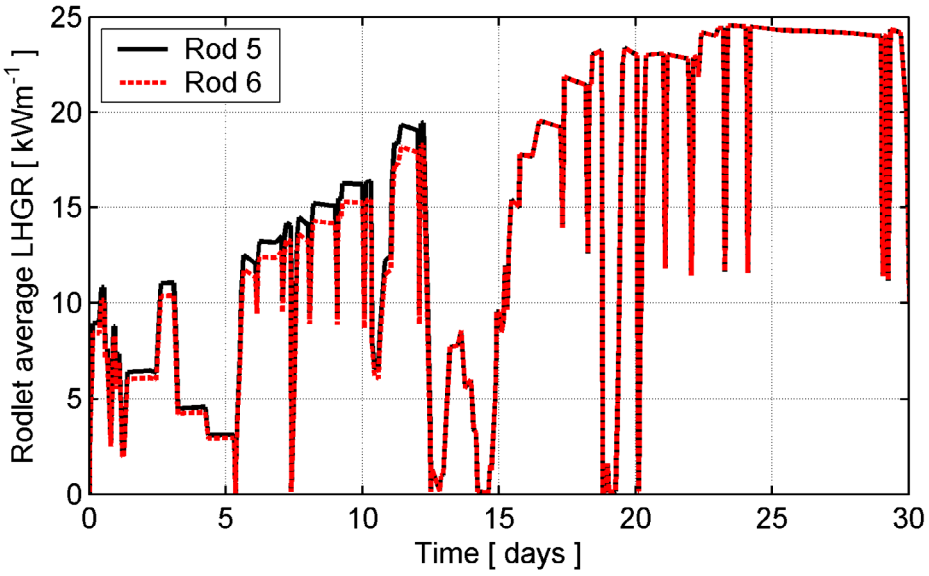

Figure A.7: Rodlet power histories for the IFA-629.3 experiment in the Halden reactor.

Appendix B: Fuel densification model in FRAPCON-3.3

The fuel densification model used in FRAPCON-3.3 is a slight modification of the FUDENS model in the MATPRO material properties library (Hagrman et al., 1981). The model is empirical, and correlates fuel densification with burnup. The model also requires a user-supplied value for the maximum densification that can be reached in the considered fuel material. The correlation reads

$$\varepsilon(B) = \varepsilon_m + e^{-3(B-B_o)} + 2e^{-35(B-B_o)}, \quad \text{(B.1)}$$

where ε [%] is the linear strain caused by densification, ε_m is the maximum densification strain, and B [MWd(kgHM)$^{-1}$] is the fuel burnup. It should be remarked that both ε and ε_m in eq. (B.1) are negative numbers, i.e. they correspond to shrinkage of the material.

The maximum densification is calculated from the relative change of density ($\Delta\rho/\rho$), measured in a standardized out-of-reactor re-sintering test at a constant temperature of 1700 °C under 24 hours. In FRAPCON-3.3, $\Delta\rho$ and ρ are supplied as input to the densification model, and ε_m is calculated from

$$\varepsilon_m = \frac{100}{3}\frac{\Delta\rho}{\rho}. \quad \text{(B.2)}$$

If data from re-sintering tests are unavailable, ε_m is instead estimated from

$$\varepsilon_m = -C_5\left(\frac{100 - f_\rho}{T_s - 1453}\right), \quad \text{(B.3)}$$

where f_ρ is the fuel density in percent of its theoretical value and T_s [K] is the fuel sintering temperature. If T_s is not provided as input by the user, a default value of 1873 K is used. The coefficient C_5 in eq. (B.3) is 22.2 for fuel temperatures up to 1000 K, and 66.6 otherwise. Hence, the maximum densification is assumed to increase discontinuously by a factor of three at 1000 K, which is surely a simplistic modelling approach. Finally, B_o in eq. (B.1) is determined from the initial condition $\varepsilon(B = 0) = 0$. Equation (B.1) is plotted for three different values of ε_m in figure B.1. Densification data for MIMAS AUC MOX fuel by Caillot et al. (1997) are included in the figure for comparison. These data pertain to fuel, operated in pressurized water reactors at linear heat generation rates between 12 and 22 kWm^{-1}.

Equation (B.1) is a slight modification of a correlation proposed by Rolstad et al. (1974), based on measurements of fuel pellet column length changes in early Halden reactor experiments on UO_2 fuel. Such length changes are controlled by the material behaviour mainly at the shoulder of the fuel pellet, where the temperature is fairly low and thermal contributions to the densification are negligible. Temperature is therefore not considered in the correlation. Equation (B.1) is in FRAPON-3.3 applied to calculate the local densification in each mesh point of the fuel pellet column, and the total fuel densification is calculated by integration of the local strains over the fuel volume.

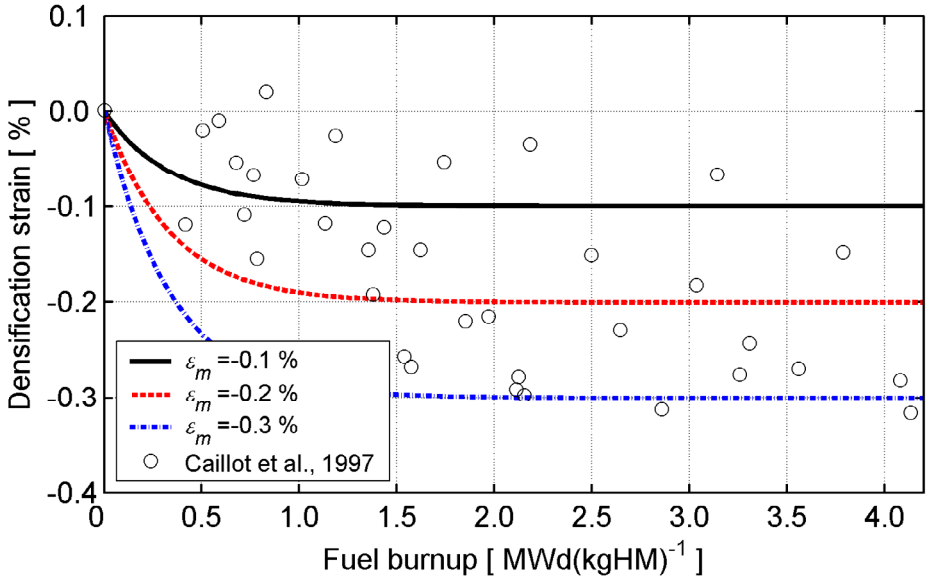

Figure B.1: The FRAPCON-3.3 densification model in eq. (B.1), plotted for three different values of the maximum densification strain, ε_m. Measured data for MIMAS AUC MOX fuel by Caillot et al. (1997) are included for comparison.

It should be remarked that the densification model is fitted to data for UO_2 fuel, but used also for MOX fuel. It is thus assumed that any differences in densification behaviour between fuel materials are captured by the parameter ε_m, which is provided as input to the model. The data for MIMAS AUC MOX fuel presented in figure B.1 suggest that this type of fuel would in fact densify at a slower rate than UO_2, but additional data are needed to confirm this observation.

As already mentioned, ε_m is supposed to be determined from an out-of-reactor isothermal re-sintering test. It has been questioned to what extent such a test can be considered as predictive with regard to in-reactor fuel densification, since the densification mechanisms are different under irradiation (Garcia et al., 2000).

www.ski.se

STATENS KÄRNKRAFTINSPEKTION
Swedish Nuclear Power Inspectorate

POST/POSTAL ADDRESS SE-106 58 Stockholm
BESÖK/OFFICE Klarabergsviadukten 90
TELEFON/TELEPHONE +46 (0)8 698 84 00
TELEFAX +46 (0)8 661 90 86
E-POST/E-MAIL ski@ski.se
WEBBPLATS/WEB SITE www.ski.se